

DEVELOPMENT OF NOVEL, CNS PENETRANT MGLU<sub>3</sub> SELECTIVE NEGATIVE  
ALLOSTERIC MODULATOR PROBES DERIVED FROM A CLOSELY RELATED  
MGLU<sub>5</sub> POSITIVE ALLOSTERIC MODULATOR

BY

JOSHUA ANDREW BRUNER

Thesis

Submitted to the Faculty of the  
Graduate School of Vanderbilt University

In partial fulfillment of the requirements

For the degree of

MASTER OF SCIENCE

in

Chemistry

May, 2012

Nashville, Tennessee

Approved:

Professor Craig Lindsley

Professor Gary Sulikowski

To my parents, Pam and Lewis, for always being supportive

and

To my MRB IV 12<sup>th</sup> floor friends, who never let me have a dull day in lab

## ACKNOWLEDGMENTS

First, I would like to thank my advisor, Professor Craig Lindsley. He has always provided terrific insight into my project and job search. I would also like to thank professor Gary Sulikowski, who in class and as the second half of my committee has taught me a myriad of organic chemistry lessons that provided a superb foundation for my master's studies. In addition, I would like to thank the VICB for funding my research.

My grandmother, Elsie, has always instilled in me a love for science. From building model rockets to always asking me the details of what I had learned during my school day, I would like to thank her for teaching me how to explain what I was learning. My parents, Pam and Lewis, have always been infinitely supportive of all my decisions in life, especially in deciding to pursue a graduate degree at Vanderbilt University. Without them, I would not be the person I am today. In the same regard, my sisters, Jenifer and Brittany, have always been there for me and have shaped me into the middle sibling I have become.

It would be a complete oversight to not mention my friends from North Carolina State University who have always been there for me through thick and thin. Luckily, I have also made many great friends here at Vanderbilt. My fellow bay members, Sydney, Margie, and Mark (and honorary member Matt), and good friends Brandon, Kris, and Mike, have made my time at Vanderbilt something I would not trade for the world.

## TABLE OF CONTENTS

	Page
DEDICATION .....	ii
ACKNOWLEDGMENTS .....	iii
LIST OF TABLES .....	vi
LIST OF FIGURES .....	vii
LIST OF SCHEMES .....	viii
Chapter	
I. INTRODUCTION.....	1
1.1 Glutamate receptors – Introduction and structure.....	1
1.2 Expression and function of mGlu <sub>3</sub> .....	4
1.3 Allosteric ligands for mGlu <sub>3</sub> .....	6
1.4 Origin of mGlu allosteric modulators; the MPEP chemotype.....	8
1.5 Allosteric modulation of mGlu <sub>3</sub> .....	10
Notes on figures, tables, and compound numbering.....	13
II. LEAD OPTIMIZATION AROUND DISTAL PHENYL RING .....	14
2.1 Synthesis of analogues around the distal phenyl ring.....	14
2.2 Pharmacological testing of compound 9l (VU0457299).....	16
2.3 Chapter summary .....	18
III. LEAD OPTIMIZATION AROUND AMIDE BOND.....	20
3.1 Synthesis of analogues around the proximal amide bond.....	20
3.2 Structure Activity Relationships (SAR) .....	21
3.3 <i>In vitro</i> and <i>in vivo</i> pharmacological testing of 19 (VU0463597).....	24
3.4 Analog development using Grignard additions .....	28
3.5 Analog development via <i>O</i> -alkylation of VU0092273.....	29
3.6 Analog development via reductive aminations.....	30
3.7 Chapter summary .....	32

IV. CURRENT EFFORTS AND FUTURE DIRECTIONS.....	33
4.1 Current efforts utilizing molecular switches.....	33
4.2 Future efforts aimed at improving pharmacokinetics of mGlu <sub>3</sub> probe .....	36
4.3 Chapter summary .....	38
V. EXPERIMENTAL .....	39
5.1 Methods and Materials.....	39
Appendix	
A. REFERENCES CITED .....	54
B. COMPOUND STRUCTURES.....	57

## LIST OF TABLES

	Page
<i>Chapter II</i>	
Table	
1. Selected analogs from Sonagashira coupling library .....	16
 <i>Chapter III</i>	
Table	
1. Structure and activity of analogs <b>14</b> .....	21
2. Representative reductive amination products <b>33</b> and activities at mGlu <sub>2</sub> and mGlu <sub>3</sub> .....	31

## LIST OF FIGURES

	Page
<i>Chapter I</i>	
Figure	
1. Structural topology of typical orthosteric and allosteric sites of mGlu <sub>5</sub> .....	3
2. Cascade of agonist binding to group II mGlu <sub>5</sub> .....	5
3. Structures of mGlu <sub>5</sub> allosteric modulators MPEP and MTEP .....	8
4. The use of molecular switches to modify the mode of pharmacology within mGlu <sub>5</sub> .....	10
5. Structures of mGlu <sub>3</sub> NAMs RO4491533 ( <b>1</b> ) and LY2399575 ( <b>2</b> ).....	11
6. PAM (mGlu <sub>5</sub> ) and NAM (mGlu <sub>3</sub> ) activity of VU0092273 ( <b>5</b> ).....	12
 <i>Chapter II</i>	
Figure	
1. Library optimization for VU0092273 ( <b>5</b> ).....	15
2. Activity of VU0402222 ( <b>9e</b> ) and VU0457299 ( <b>9l</b> ).....	18
 <i>Chapter III</i>	
Figure	
1. Structure of VU0092273.....	22
2. Structure of VU0459730 ( <b>15</b> ) and “PAM-like” response in GIRK assay .....	23
3. <i>In vitro</i> molecular pharmacology characterization of <b>12</b> (VU0463597) .....	25
4. Metabolite ID studies showed the major metabolite of <b>19</b> is phenol <b>21</b> , via O-dealkylation of the methyl ether .....	27

## LIST OF SCHEMES

	Page
<i>Chapter II</i>	
Scheme	
1. Reagents and conditions for the synthesis of <b>9</b> .....	15
 <i>Chapter III</i>	
Scheme	
1. Synthesis of 4-OMePh scaffold and general amide coupling.....	20
2. Synthesis and activities of (R)- <b>19</b> and (S)- <b>20</b> .....	24
3. Synthesis of O-demethylation product <b>21</b> .....	27
4. Synthesis of trifluoromethyl ether analog <b>26</b> .....	28
5. Synthesis of Grignard products <b>28-29d</b> .....	29
6. Synthesis of O-alkylation analogs <b>30-31d</b> .....	30
7. Synthesis of generic amine <b>33</b> via reductive amination.....	31
 <i>Chapter IV</i>	
Scheme	
1. Synthesis of pyridinyl analogs VU0464192 ( <b>36</b> ), VU0464193 ( <b>39</b> ), and <b>42</b> from brominated nicotinic and picolinic acid derivatives.....	34
2. Synthesis of pyrimidines <b>45</b> and <b>48</b> and pyrazine <b>51</b> .....	35
3. Alternative route to arrive at pyrimidines <b>45</b> and <b>48</b> and pyrazine <b>51</b> .....	36



4. Proposed route to generic substituted alkyl ether <b>61</b> .....	36
5. Route to obtain benzyl ether <b>66</b> .....	37

# CHAPTER I

## INTRODUCTION

mGluRs have been proven to be therapeutic targets for a range of psychiatric disorders including schizophrenia, substance abuse, anxiety disorders, and depression. Schizophrenia, especially, is a complex mental disorder that affects approximately 1% of the world's population.<sup>1</sup> The core symptoms of the disorder are subdivided into four distinct groups including positive, negative, cognitive, and affective<sup>2</sup>. The NMDA receptor hypofunction hypothesis is generally the favored pathophysiological model for the disease mechanism for schizophrenia. As a result, multiple approaches to enhance the glutamate/NMDA system continue to be pursued as a means to ameliorate the major symptom dimensions of the disease.<sup>3,4</sup> Recently, several findings have suggested that group II mGluRs are involved in the pathophysiology of schizophrenia especially. However, little is known of whether this group II mGluR involvement is attributed to mGlu<sub>2</sub> or mGlu<sub>3</sub>.<sup>5</sup> As a result, molecular probes that selectively target mGlu<sub>3</sub> are necessary to determine its involvement in disease pathogenesis.

### **1.1 Glutamate receptors – Introduction and structure**

Glutamate is the primary excitatory neurotransmitter in the human central nervous system.<sup>2</sup> It is essential in many physiological processes and affects a diverse group of receptors including ionotropic and metabotropic glutamate receptors. The ionotropic glutamate receptors (iGluRs) are ligand-gated ion channels and are responsible for fast

synaptic transmission. In the presence of an agonist, these channels are permeable to cations. Ionotropic receptors consist of a tetramer of subunits and are categorized into three subtypes based on pharmacological and electrophysiological data. These include  $\alpha$ -amino-3-hydroxy-5-methyl-4-isoxazole propionate (AMPA) receptors, kainite (KA) receptors, and N-methyl-D-aspartate (NMDA) receptors. Ionotropic glutamate receptors contain an extracellular amino terminal domain, bi-lobed agonist binding domain, and a pore forming membrane-residing domain, which forms a reentrant loop entering from and exiting the cytoplasm.<sup>6</sup> The metabotropic glutamate receptors (mGlu) belong to G-protein coupled receptor (GPCR) family C. Eight mGlu have been cloned, sequenced and assigned to three groups based on their sequence homology, pharmacology, and coupling to effector mechanisms.<sup>6,7</sup> These include: group I – mGlu<sub>1</sub> and mGlu<sub>5</sub>; group II – mGlu<sub>2</sub> and mGlu<sub>3</sub>; and group III – mGlu<sub>4</sub>, mGlu<sub>6</sub>, mGlu<sub>7</sub> and mGlu<sub>8</sub>. mGlu within the same group maintain approximately 70% homology while intergroup homology is maintained at about 45%.<sup>8</sup> These receptors are similar in that each contains an intracellular, an extracellular, and a 7-transmembrane domain each of which is shown in Figure 1.<sup>9,10</sup>

## Typical orthosteric and allosteric sites of mGluRs

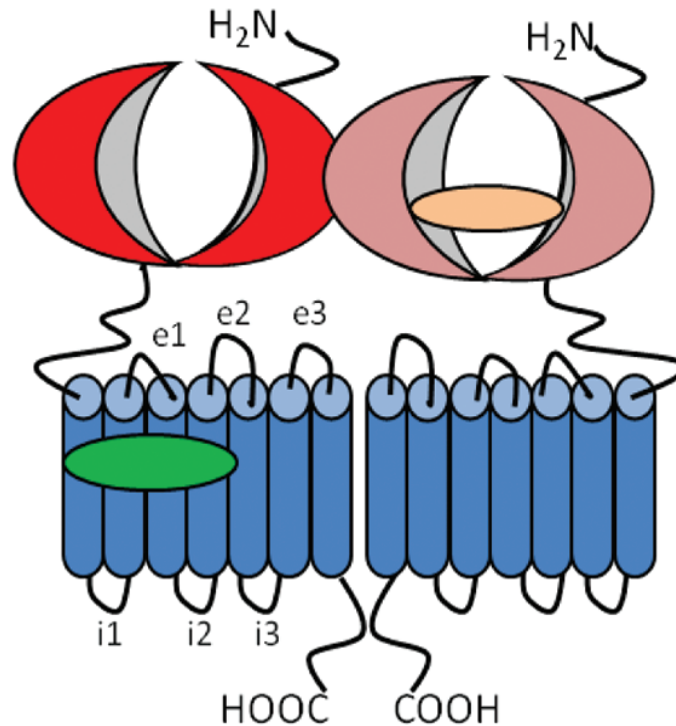


**Figure 1.** Structural topology of typical orthosteric and allosteric sites of mGluR highlighting representative orthosteric and allosteric ligands by the beige and green ovals respectively (Melancon, et al 2012).

The carboxy-terminal intracellular domain of mGluR is highly variable and is the location of the binding site for a variety of intracellular proteins involved in receptor signaling, receptor desensitization, and receptor targeting.<sup>6</sup> The extracellular domain consists of the venus-flytrap domain and the cysteine-rich domain. The venus-flytrap contains the highly conserved orthosteric-binding site, which consists of two large globular domains and a connecting hinge region. The two globular domains are capable of folding together in order to bind glutamate and other orthosteric ligands. The cysteine rich domain of the extracellular segment connects the venus-flytrap domain to the

transmembrane domains. The nineteen cysteine residues in this region are conserved among all mGlu<sub>3</sub>, and it is thought that these residues play a key role in three-dimensional structure, intramolecular transduction, and receptor dimerization. In addition to carboxy-terminal intracellular domain and the extracellular domain, all family C GPCRs contain a 7-transmembrane domain (7TMD), which consists of seven membrane spanning  $\alpha$ -helices that are connected via short intra- and extracellular loops.<sup>6</sup>

mGlu<sub>3</sub> exist exclusively as homodimers that are held together by their extracellular domains through disulfide bonds in addition to the hydrophobic interface of the constituents. In the inactive state, the extracellular domains of the constituents exist in a physically separated and open confirmation. Upon ligand binding the domains close together forming the homodimer. Intracellular signal transduction is initiated by the rotation of the extracellular domains in relation to one another upon ligand binding which leads to the stabilization of the transmembrane domain.<sup>6</sup>

## 1.2 Expression and function of mGlu<sub>3</sub>

mGlu<sub>3</sub> consists of 879 amino acids and has a predicted molecular weight of approximately 95 kDa. Its intracellular domain couples via G<sub>i</sub> and G<sub>o</sub> to inhibit adenylate cyclase, which is responsible for the formation of cyclic adenosine monophosphate (cAMP). The intracellular C-terminal tail also interacts with a number of regulatory proteins.<sup>10</sup> This cascade of events has been shown to generate secondary messengers and activation of extracellular signal-regulated kinase 1/2 (ERK1/2) and phosphoinositide 3-kinase (PI3K) (**Figure 2**).<sup>11</sup>

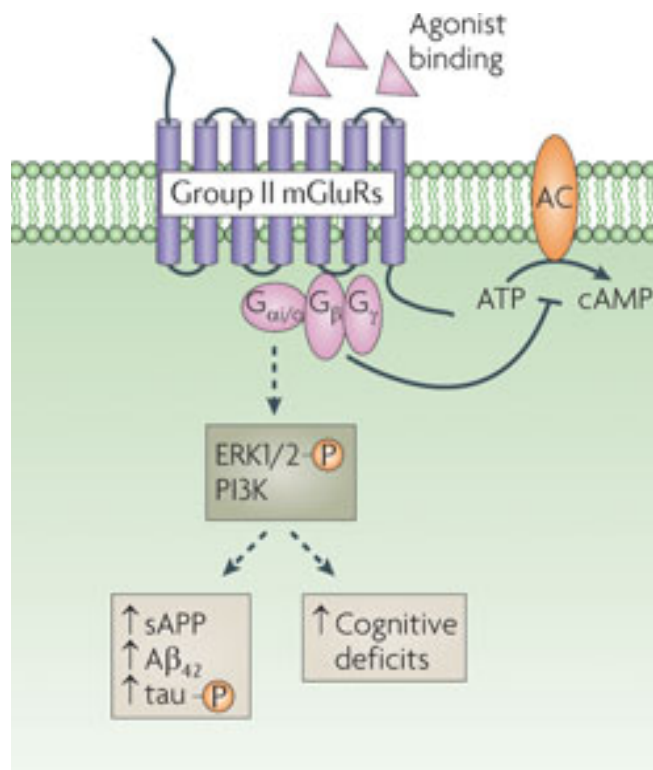


**Figure 2.** Cascade of agonist binding to group II mGluR leading to G-protein inhibition of adenylyl cyclase and the production of cAMP from ATP. The binding of an agonist to group II mGluR leads to an increase in amyloid- $\beta_{42}$  generation, tau phosphorylation and an exacerbation of the cognitive deficits in an AD mouse model via  $G_{\alpha i/o}$  signaling through ERK1/2 and PI3K (Thathia and Strooper 2011)

In general, the group II mGluR play an important role in synaptic plasticity, which directly effects learning and memory among other things. The effects of group II mGluR occur primarily presynaptically via their inhibition of glutamate release. These effects can also be ascribed to the inhibition of non-vesicular glutamate release from glia. It is suggested that mGlu<sub>3</sub> is involved with regulating non-synaptic glutamate since it is localized away from active synaptic zones.<sup>5</sup>

Results from mGlu<sub>3</sub> expression and function studies largely overlap between human and rat studies. mGlu<sub>3</sub> in humans is localized to neurons in the cerebral cortex, dentate gyrus granule cells, Golgi and basket/stellate cells in the cerebellum and neurons of the thalamic reticular nucleus. Species differences include the finding that expression in subcortical white matter and reticular thalamic nucleus is much less prominent in humans than in rodents.<sup>5</sup>

Few compounds have shown selectivity within group II mGlu<sub>s</sub>. Particularly only selective mGlu<sub>2</sub> positive allosteric modulators (PAMs) have been identified.<sup>12</sup> One exception is the low-affinity endogenous agonist N-acetylaspartylglutamate (NAAG).<sup>5</sup> Selectivity of available antibodies has also been too poor to target one group II mGlu over another. Therefore, the individual roles of mGlu<sub>2</sub> and mGlu<sub>3</sub> have been difficult to evaluate and are poorly understood. Thus, it is necessary to develop selective analogs to study each receptor individually. This could be accomplished by developing allosteric ligands that bind outside the highly conserved orthosteric binding site, taking advantage of regions with reduced homology.

### **1.3 Allosteric ligands for mGlu<sub>s</sub>**

G-protein-coupled receptors (GPCRs) have proven themselves as successful drug targets; however, selective ligands have yet to be developed for the majority of these receptors. Several issues have slowed the successful development of highly selective ligands for GPCRs. These include that the orthosteric binding sites across families of GPCRs are highly conserved and that native ligands for orthosteric sites of many GPCRs have properties that are incompatible with commonly used scaffolds in small-molecule

drug discovery.<sup>12</sup> Alternatively, one could create allosteric modulators that bind outside the highly conserved orthosteric region to target the individual subtypes of GPCRs. This strategy would allow for one to tune selectivity where sequence homology is much lower in the allosteric region of the receptors (**Figure 1**).<sup>8</sup>

Small molecules that target allosteric regions of GPCRs could potentiate or inhibit activation of the receptor by its native ligand. Upon binding, allosteric GPCR modulators can exhibit several different pharmacological properties. These include: affinity modulation, efficacy modulation, and agonism/inverse agonism. Affinity modulation involves a change in the association and/or dissociation rate of an orthosteric ligand with its binding pocket, resulting from a conformational change caused by an allosteric modulator. Efficacy modulation, in the regard of allosteric modulation, is an alteration of the intracellular responses leading to a change in the signaling capacity within the cascade. Finally, agonism is the perturbation of a signaling cascade in a positive manner, while inverse agonism is the same in a negative way. mGlu<sub>s</sub> are a prime examples of GPCRs that exhibit high sequence homology within their orthosteric binding pockets. Because of this binding pocket homology and the fact that little is known about the true pathology of many CNS disorders and how their pathology may be affected by modulating mGlu<sub>s</sub>, it is desirable to develop probes that target each subtype of the mGlu<sub>s</sub> selectively.<sup>12</sup>

Highly subtype selective allosteric ligands (both positive and negative allosteric modulators, PAMs and NAMs respectively) have been developed for mGlu<sub>1</sub>, mGlu<sub>2</sub>, mGlu<sub>4</sub>, and mGlu<sub>5</sub>.<sup>8, 12-18</sup> Until now, in regard to Group II ligands, only selective mGlu<sub>2</sub> PAMs have been discovered. Most Group II ligands do not discriminate between mGlu<sub>2</sub>



and mGlu<sub>3</sub> in lieu of the fact that these two receptors share divergent expression and functional differences.<sup>18-21</sup> Due to the lack of selective small molecule probes for the Group II mGlu<sub>s</sub> it has been difficult to discern distinct pharmacological roles for mGlu<sub>3</sub>. However, numerous studies suggest mGlu<sub>3</sub> is involved in glial-neuronal communication and may have therapeutic potential for the treatment of schizophrenia, alzheimer's disease, and depression, therefore, making it an ideal target for the development of selective allosteric modulators.<sup>8, 12 13, 19, 23-25</sup>

#### 1.4 Origin of mGlu allosteric modulators; the MPEP chemotype

The discovery of SIB-1893 and 2-Methyl-6-(phenylethynyl)pyridine (**1**, MPEP) (**Figure 3**) in the late 1990s by scientists at SIBIA Neurosciences and Novartis, respectively, began the blossoming of selective allosteric modulators of mGlu<sub>s</sub>.<sup>26,27</sup> MPEP was initially reported as a potent, selective, and systemically active antagonists of mGlu<sub>5</sub>. This antagonism comes with limited activity at mGlu<sub>1</sub>, Group II, and Group III receptors as well as at ionotropic glutamate receptors.<sup>27</sup>

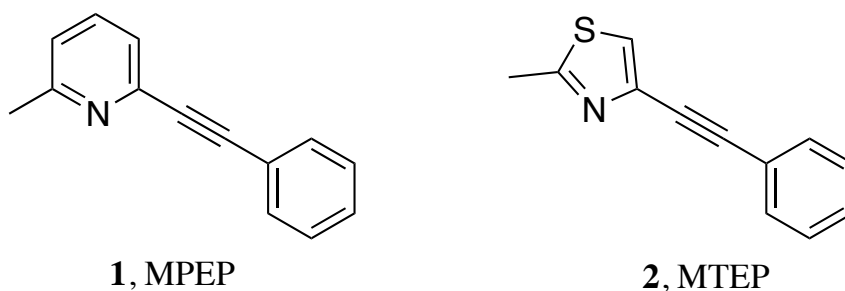


**Figure 3.** Structures of mGlu<sub>5</sub> allosteric modulators MPEP and MTEP

Due to several shortcomings of MPEP as an *in vivo* therapeutic agent such as off-target activity and poor aqueous solubility, it was necessary to discover new antagonists that offered improved pharmacological properties. This effort led to the discovery of the more potent mGlu<sub>5</sub> antagonist by Merck & Co., 3-((2-Methyl-4-thiazolyl)ethynyl)pyridine (**2**, MTEP).<sup>28</sup> MTEP (**Figure 3**) was initially reported as a potent and selective antagonist of mGlu<sub>5</sub> with fewer off-target effects than MPEP. *In vivo* rat models also demonstrated that MTEP was more potent in receptor occupancy studies as well as in the fear-potentiated startle model of anxiety.<sup>28</sup>

With MPEP and MTEP in hand, and a more thorough understanding of how allosteric modulation could be utilized to affect mGlu<sub>5</sub>, a plethora of “MPEP-like” compounds have been reported by our group and others that have high propensity of displaying “molecular switches”. This molecular switch phenomena is described as a modulation in activity or even the mode of pharmacology by single molecular changes within a scaffold.<sup>29-32</sup> The use of molecular switches as they pertain mGlu<sub>5</sub> modulation can be seen in Figure 4.<sup>32</sup> The MPEP-chemotype of allosteric modulators has demonstrated this phenomena across mGlu<sub>5</sub>, and will be the foundation of our studies targeting mGlu<sub>3</sub>.

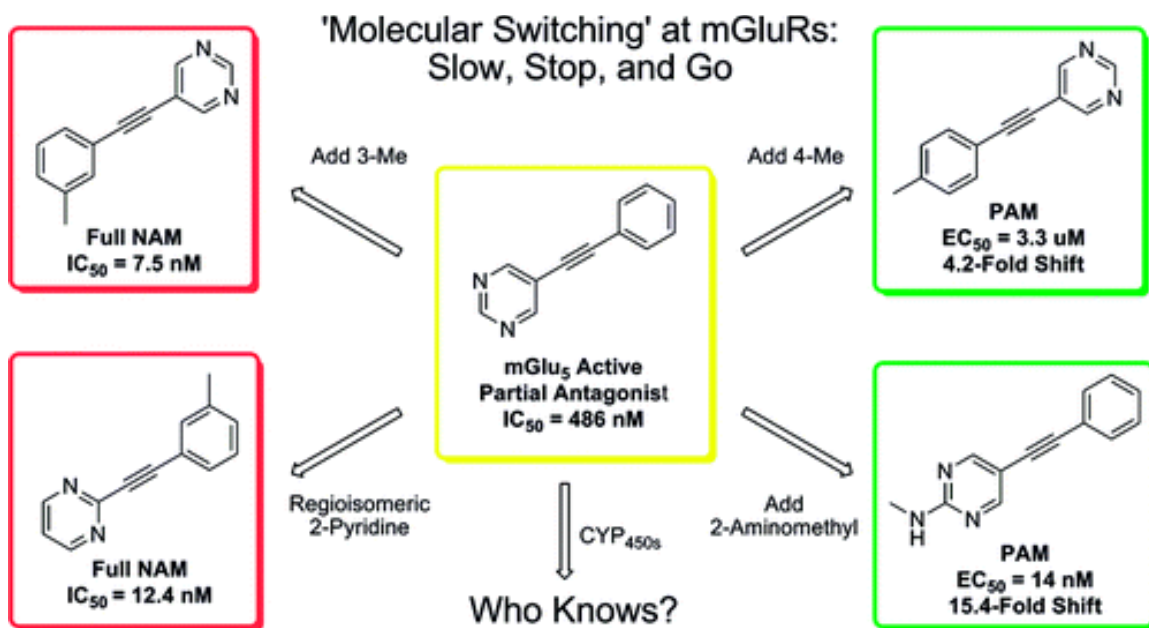
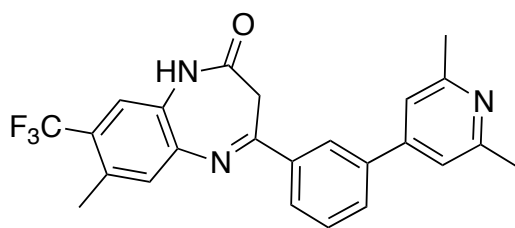


**Figure 4.** The use of molecular switches to modify the mode of pharmacology within mGlu<sub>5</sub> (Wood 2011)

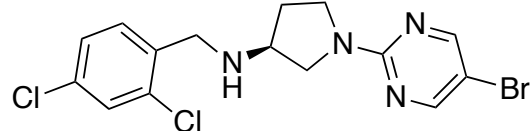
### 1.5 Allosteric modulation of mGlu<sub>3</sub>

To date, only two mGlu<sub>3</sub> NAMs have been reported (**Figure 5**).<sup>33, 34</sup> The first, reported by Addex, was RO4491533 (**3**), a dual mGlu<sub>2</sub>/mGlu<sub>3</sub> NAM (mGlu<sub>2</sub> IC<sub>50</sub> = 296 nM, mGlu<sub>3</sub> IC<sub>50</sub> = 270 nM) based on a benzodiazepine nucleus that was efficacious in preclinical cognition and depression models.<sup>33</sup> At the same time, Lilly disclosed LY2389575 (**4**), as a selective mGlu<sub>3</sub> NAM,<sup>34</sup> however, in our hands, **4** is only ~4-fold selective for mGlu<sub>3</sub> over mGlu<sub>2</sub> (mGlu<sub>2</sub> IC<sub>50</sub> = 17 mM, mGlu<sub>3</sub> IC<sub>50</sub> = 4.2 mM) when measuring native coupling of these receptors to G protein inwardly rectifying potassium (GIRK) channels via thallium flux.<sup>35</sup> Thus, there is a critical need for potent and selective mGlu<sub>3</sub> ligands.



**3**, RO4491533

mGlu<sub>2</sub> IC<sub>50</sub> = 296 nM  
mGlu<sub>3</sub> IC<sub>50</sub> = 270 nM



**4**, LY2399575

LY mGlu<sub>2</sub> IC<sub>50</sub> > 12.5 μM  
LY mGlu<sub>3</sub> IC<sub>50</sub> = 190 nM

VU mGlu<sub>2</sub> IC<sub>50</sub> = 17 μM  
VU mGlu<sub>3</sub> IC<sub>50</sub> = 4.2 μM

**Figure 5.** Structures of mGlu<sub>3</sub> NAMs RO4491533 (1) and LY2399575 (2), both dual mGlu<sub>2</sub>/mGlu<sub>3</sub> NAMs.

In the absence of an HTS campaign to identify novel mGlu<sub>3</sub> NAMs, we elected to take advantage of the propensity of certain mGlu<sub>5</sub> PAM chemotypes to induce molecular switches and easily modulate the mode of pharmacology or mGlu subtype selectivity with subtle structural alteration.<sup>29-32, 36, 37</sup> One such chemotype that we, and others, have reported on with a high propensity for displaying ‘molecular switches’ is represented by VU0092273 (**5**). Compound **5** a very potent MPEP-site mGlu<sub>5</sub> PAM (**Figure 6**) and highly selective across six of the mGlu<sub>s</sub>. However, **5** possessed weak mGlu<sub>3</sub> NAM activity (IC<sub>50</sub> ~ 10 mM, inhibits EC<sub>80</sub> by 72%) providing a lead compound from which to develop a potent and selective mGlu<sub>3</sub> NAM.

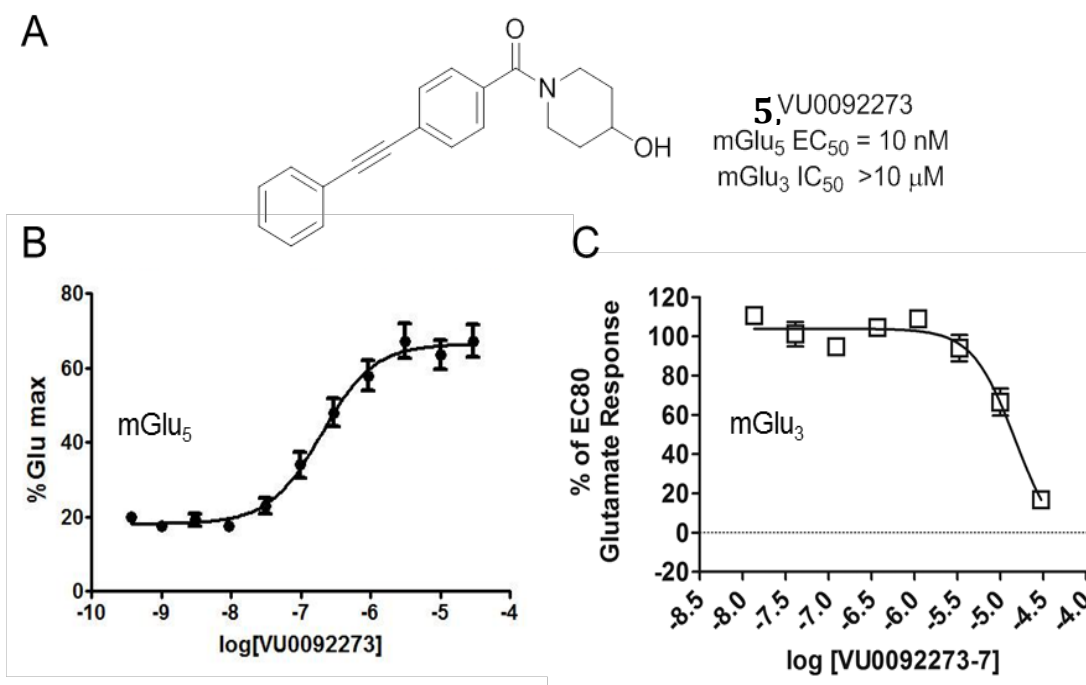


**Figure 6.** PAM (mGlu<sub>5</sub>) and NAM (mGlu<sub>3</sub>) activity of VU0092273 (**5**) (A) Structure of VU0092273 (**5**), a potent mGlu<sub>5</sub> PAM (EC<sub>50</sub> = 10 nM). (B) mGlu<sub>5</sub> PAM concentration-response curve (CRC) in presence of an EC<sub>20</sub> of glutamate. (C) mGlu<sub>3</sub> antagonist CRC. **5** displayed weak NAM activity at mGlu<sub>3</sub> (IC<sub>50</sub> >10 mM, inhibits EC<sub>80</sub> ~ 72%)

### **Notes on figures, tables, and compound numbering**

Throughout the remaining Chapters, all figure and table numbering is specific to each Chapter. Put differently, each Chapter's figure and table numbering begins with "1". Similarly, compound numbering formats and nomenclature is specific for each Chapter. Arbitrary numbering (e.g. Compound **1** or **(1)**) is used interchangeably throughout each Chapter. These are used in place of the VU registration codes (e.g. VU0075630) in order to increase the ease and readability and to reduce space. Table 1 in the Appendix contains the Thesis numbering and VU registration code listed for each compound (by Thesis numbering) to allow for ease in requesting compounds from universal storage or referencing laboratory notebooks.

## CHAPTER II

### LEAD OPTIMIZATION AROUND DISTAL PHENYL RING

#### 2.1 Synthesis of analogues around the distal phenyl ring

Initial optimization efforts were focused around the distal phenyl ring. As we have previously reported, due to the steep nature of allosteric modulator SAR (especially in series prone to ‘molecular switches’), we pursued a targeted iterative parallel synthesis approach for the chemical optimization of **5**.<sup>7,8</sup> Creating a library using this approach stems from the idea of generating fewer, but specifically designed compounds based on a desired structural motif and physiochemical properties. In turn, a balance is established with the ability to synthesize targeted libraries while highly optimized biological test systems allow us to produce an abundance of data. Ultimately this creates an efficient workflow that greatly reduces the length of timelines in medicinal chemistry projects.<sup>38</sup>

Previous work in this scaffold (**5**) indicated that mGlu<sub>5</sub> PAM activity could be greatly diminished with substitution other than fluorine on the distal aryl ring, as well as with modifications to the amide moiety.<sup>29</sup> Therefore, our first generation library design (**Figure 1**) initially held the 4-hydroxypiperidine amide constant, while surveying a diverse array of functionalized aryl/heteroaryl rings as well as other aliphatic groups. Once mGlu<sub>3</sub>-preferring modifications were identified, these were maintained and an amide scan was performed to both improve mGlu<sub>3</sub> NAM activity while eliminating mGlu<sub>5</sub> PAM activity.

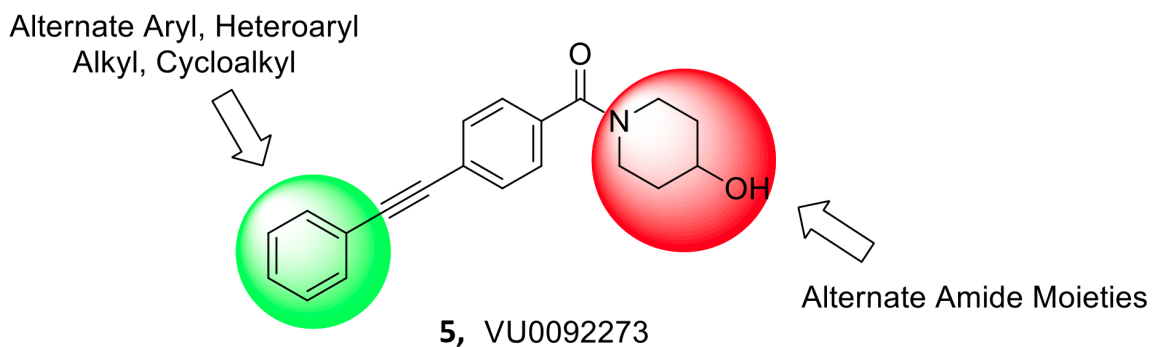
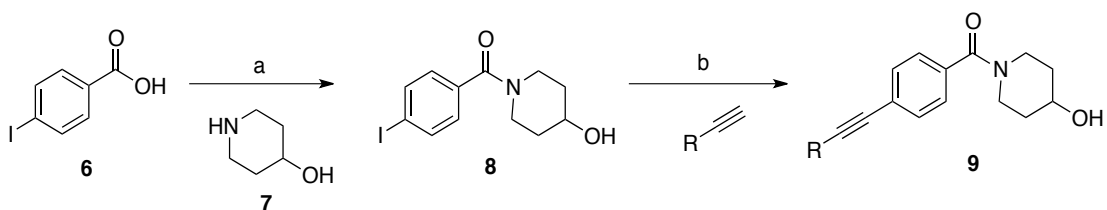


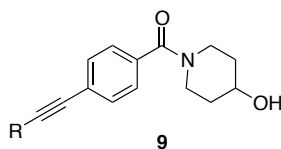
**Figure 1.** Library optimization strategy for VU0092273 (**5**) to improve mGlu<sub>3</sub> NAM activity while simultaneously eliminating mGlu<sub>5</sub> PAM activity.

Our first 48-member library was prepared as shown in Scheme 1, and purified, to >98% purity, by reverse phase chromatography.<sup>39</sup> Commercially available 4-iodobenzoic acid **6** was coupled to 4-hydroxypiperidine **7**, under standard EDC/HOBt conditions, to provide amide **8** in 95% yield. Once in hand, **8** underwent 48 microwave-assisted Sonogashira coupling reactions with a diverse array of functionalized terminal acetylenes to provide analogs **9** (Scheme 1). Selected analogs are shown in Figure 1 and an exhaustive list of analogs can be found in appendix B.



**Scheme 1.** Reagents and conditions: (a) EDC, DMAP, DCM, DIPEA, 95%; (b) 20% CuI, 5% Pd(PPh<sub>3</sub>)<sub>4</sub>, 48 acetylenes (1.1 equiv.), DMF, DIEA, 60 °C, 1 h, 15-90%.



**Table 1.** Selected analogs from Sonagashira coupling library

Cmpd	R	mGlu3 IC50 (μM)	%Glu min	Cmpd	R	mGlu3 IC50 (μM)	%Glu min
<b>9a</b>		10.00	4.33	<b>9h</b>		10.00	42.16
<b>9b</b>		10.00	17.54	<b>9i</b>		Inactive	76.29
<b>9c</b>		10.00	24.66	<b>9j</b>		Inactive	75.00
<b>9d</b>		Inactive	70.96	<b>9k</b>		Inactive	10.26
<b>9e</b>		10.00	54.23	<b>9l</b>		4.42	7.43
<b>9f</b>		10.00	10.82	<b>9m</b>		Inactive	83.16
<b>9g</b>		10.00	22.36	<b>9n</b>		Inactive	68.95

## 2.2 Pharmacological testing of compound 9l (VU0457299)

All 48 analogs were screened using a thallium flux assay that takes advantage of the ability of Gβγ subunits in the G<sub>i</sub> and G<sub>o</sub> heterotrimer to interact with G-protein regulated inwardly rectifying potassium channels (GIRKs). With prior knowledge that group II mGlu<sub>s</sub> are coupled to G<sub>i/o</sub>, this assay allows for the detection of various types of pharmacophores including agonists, antagonists, and allosteric modulators of group II and III mGlu<sub>s</sub>, notably including mGlu<sub>3</sub> for this research project.<sup>40</sup>

In order to test for antagonism at mGlu<sub>3</sub>, the thallium flux assay is modified by treating cells with a dose of glutamate to elicit an EC<sub>80</sub> response, followed by treatment with the test compound in hopes of observing a dose dependent decrease in thallium flux.<sup>40</sup> True to allosteric modulator SAR, 47 of 48 of the analogs were either inactive on mGlu<sub>3</sub> (IC<sub>50</sub> >10 mM) or only afforded modest inhibition (5-50% Glu Min) of the glutamate EC<sub>80</sub>. Only one compound, **9l** (VU0457299) possessing a 4-methoxyphenyl moiety, displayed mGlu<sub>3</sub> NAM potency below 10 μM (mGlu<sub>3</sub> IC<sub>50</sub> = 4.42 μM, 7.43% Glu Min) (**Figure 2**). Interestingly, the regioisomeric 2-OMe (**9m**) (**Figure 2**) and 3-OMe (**9n**) congeners were inactive as mGlu<sub>3</sub> antagonists. Lastly, the *tert*-butyl acetylene derivative **9j** was found earlier as an mGlu<sub>5</sub> PAM and showed slight activity in an mGlu<sub>3</sub> counter screen. However, this compound was resynthesized and failed to show activity in our studies. Overall, **9l** was the only active mGlu<sub>3</sub> NAM from this series of compounds and became the new lead compound to which further modifications were made.

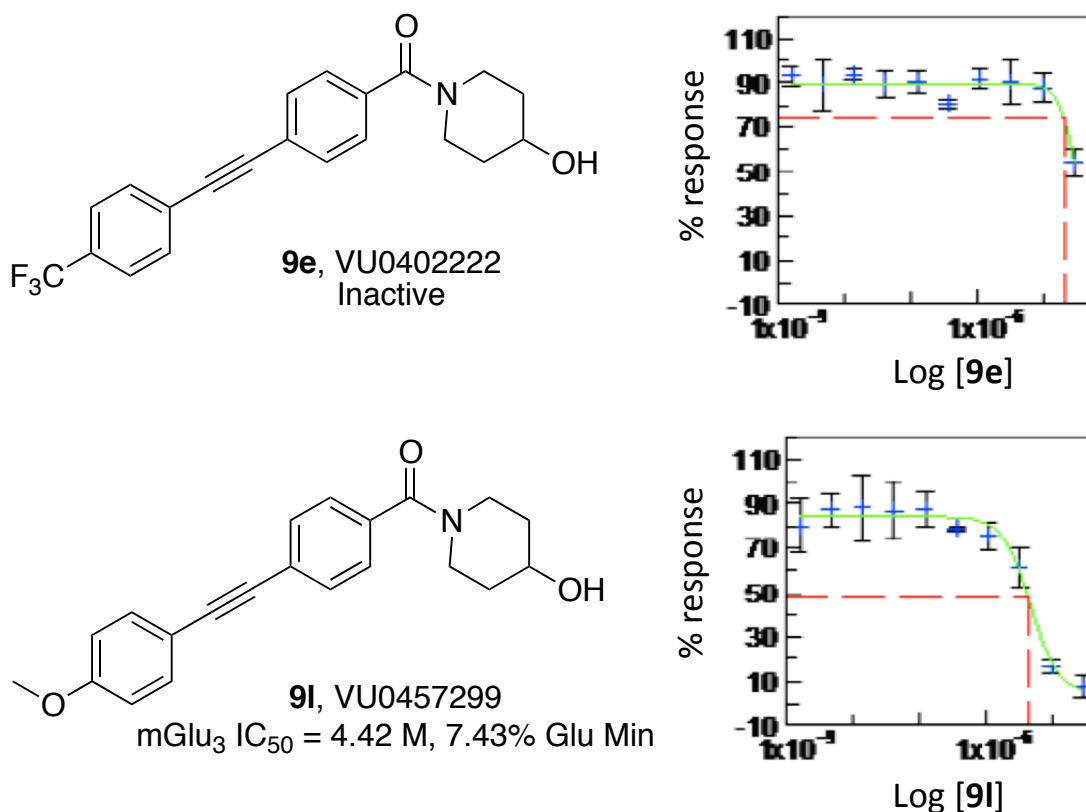


**Figure 2.** Activity of VU0402222 (**9e**) and VU0457299 (**9l**)

### 2.3 Chapter summary

With the understanding that a series of analogs based on **5** would be prone to molecular switches for altering activity, an iterative parallel synthesis approach was taken to improve on the mGlu<sub>3</sub> NAM activity of **5**. The initial synthetic strategy involved generating a 48-membered library via the means of Sonagashira couplings of iodide **8** with a series of acetylene derivatives. True to typical allosteric modulator SAR studies, 47 of 48 compounds were inactive as mGlu<sub>3</sub> NAMs. However, the *p*-methoxyphenyl analog **9l** displayed mGlu<sub>3</sub> NAM potency below 10 μM (mGlu<sub>3</sub> IC<sub>50</sub> = 4.42 μM, 7.43% Glu Min). With this data in hand, the **9l** analog then became the lead compound. We

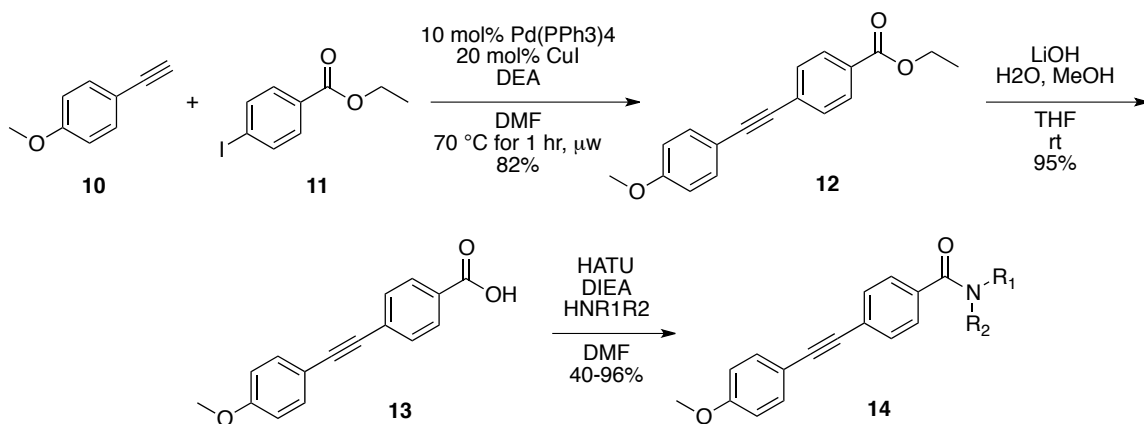
then sought to improve mGlu<sub>3</sub> NAM activity and selectivity by exploring alternative amides to be discussed in Chapter III.

## CHAPTER III

### LEAD OPTIMIZATION AROUND AMIDE BOND

#### 3.1 Synthesis of analogues around the proximal amide bond

Based on the medicinal chemistry profiling conducted in Chapter 2, varying the substituents connected via the amide bond was explored next. With the *p*-methoxy moiety from the western region of the scaffold held constant, the strategy was aimed at exploring what structural features were necessary to maintain and improve mGlu<sub>3</sub> negative allosteric modulation (NAM) activity. The goal then was to choose a suitable, selective compound with which *in vivo* studies could be used to confirm the observed *in vitro* pharmacology. An iterative analogue library synthesis approach was utilized to prepare a 48-member library. To arrive at these compounds, 4-ethynylanisole **10** first underwent a microwave-assisted Sonogashira reaction with ethyl 4-iodobenzoate **11** followed by saponification of **12** and a series of amide couplings with carboxylic acid **13** to yield the generic amide **14** in 31-75% overall yield (**Scheme 1**).



**Scheme 1.** Synthesis of 4-OMePh scaffold and general amide coupling

### 3.2 Structure Activity Relationships (SAR)

SAR within this library provided much insight to the functionalities required for mGlu<sub>3</sub> NAM activity. The initial aim was to incorporate a variety of structurally distinct moieties into this region of the molecule. Various aliphatic and aromatic amines were coupled to carboxylic acid **13** using HATU amide coupling conditions to develop the library (**Table 1**). An exhaustive list of the amines used in generating this library can be found in Appendix B.

**Table 1.** Structure and activity of analogs **14**

**14**

Cmpd	NR <sub>1</sub> R <sub>2</sub>	IC <sub>50</sub> (nM) <sup>a</sup>	%Glu Min <sup>b</sup>
9l		4.4	7.4
14a		6.3	5.4
14b		3.2	1.2
14c		5.8	0.5
14d		>10	19.5
14e		3.8	0.4
14f		6.8	1.2
14g		8.2	5.7

<sup>a</sup>Measured in mGlu<sub>2</sub> GIRK assay. <sup>b</sup>% Glu Min is the %inhibition of the compound on an EC<sub>80</sub> concentration of glutamate.

Upon screening this library in mGlu<sub>3</sub> NAM optimized G protein inwardly rectifying potassium (GIRK) channel thallium flux assay, it was evident that structural elements similar to that of **5** (VU0092273) (**Figure 1**) are required for maintaining

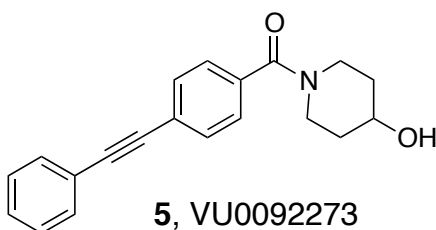


**Figure 1.** Structure of VU0092273 (**5**). This previous lead compound was used as a guide as to the structural features that need to be maintained in amide coupling library.

activity. This second library was far more productive, providing several analogs **14** with mGlu<sub>3</sub> NAM potencies below 10 mM; however, SAR was still quite steep. It became evident that polar and basic groups separated from the nitrogen of the amide bond by one to three carbons generally displayed activity (i.e. **14a,b,e**). Several aliphatic moieties that lacked polar functionalities showed no activity. The case was the same with most of the aromatic and extremely bulky amines coupled to the acetylene scaffold. Interestingly, VU0459730 (**15**) showed potential as a positive allosteric modulator (**Figure 1**). However, further testing is necessary to confirm this mechanism.

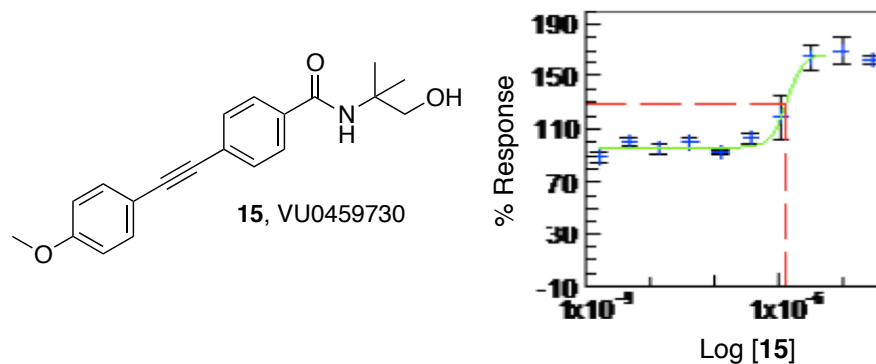
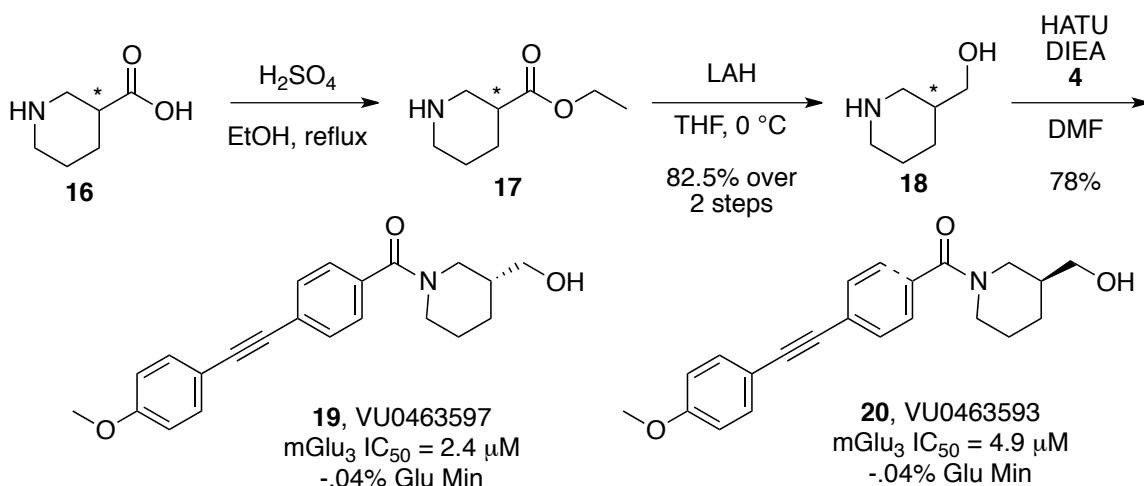


**Figure 2.** Structure of **15**, VU0459730 and "PAM-like" response in GIRK assay

The most potent mGlu<sub>3</sub> antagonist from this series of compounds was the 3-hydroxymethylpiperidine analog VU0459726 (**14e**). In addition, we found that enantioselective mGlu<sub>3</sub> inhibition was displayed by the (*S*)-piperidine carboxylic acid **14c** ( $IC_{50} = 5.8$  mM) while the (*R*)-enantiomer **14d** ( $IC_{50} \gg 10$  mM) was essentially inactive. Due to the enantioselective activity of **14c** and **14d**, it was then necessary to determine if **14e** displayed enantioselective inhibition. Following Scheme 2, both the (*R*)- and (*S*)-enantiomers of **14e**, **19** (VU0463597) and **20** (VU0463593) were synthesized and assayed in the mGlu<sub>3</sub> GIRK assay. Here, **19** ( $IC_{50} = 2.4$   $\mu$ M) was 2-fold more potent than **20** ( $IC_{50} = 4.9$   $\mu$ M), but both afforded full blockade (% Glu Mins of -0.4). Efforts now shifted towards more fully characterizing **19** (VU0463597).





**Scheme 2.** Synthesis and activities of (R)-**19** and (S)-**20**, mGlu<sub>3</sub> NAMs. Both the (R)- and (S)- enantiomers of **16** were used for the synthesis

### 3.3 *In vitro* and *in vivo* pharmacological testing of **19** (VU0463597)

We next evaluated the selectivity of **19** (VU0463597) between mGlu<sub>2</sub> and mGlu<sub>5</sub>. Utilizing our mGlu<sub>2</sub> GIRK line, the IC<sub>50</sub> was much greater than 10 mM, with the CRC not reaching baseline at this highest concentration (**Figure 2A**, triangles). Similarly, **19** had no effect on potentiating an EC<sub>20</sub> concentration of glutamate in our standard mGlu<sub>5</sub> calcium assay (**Figure 2A**, diamonds). As our calcium assays typically drive our mGlu drug discovery programs, we also evaluated **19** (VU0463597) in an mGlu<sub>3</sub> calcium assay in which mGlu<sub>3</sub> is co-expressed with the promiscuous G protein Ga15 (**Figure 2B-D**). Here, we see improved mGlu<sub>3</sub> NAM potency (IC<sub>50</sub> = 649 nM), with high selectivity versus mGlu<sub>2</sub> (~15-fold) and mGlu<sub>5</sub> in both PAM and NAM modes. Thus, we were able to optimize and develop a potent and selective mGlu<sub>3</sub> NAM starting from a very potent mGlu<sub>5</sub> PAM.

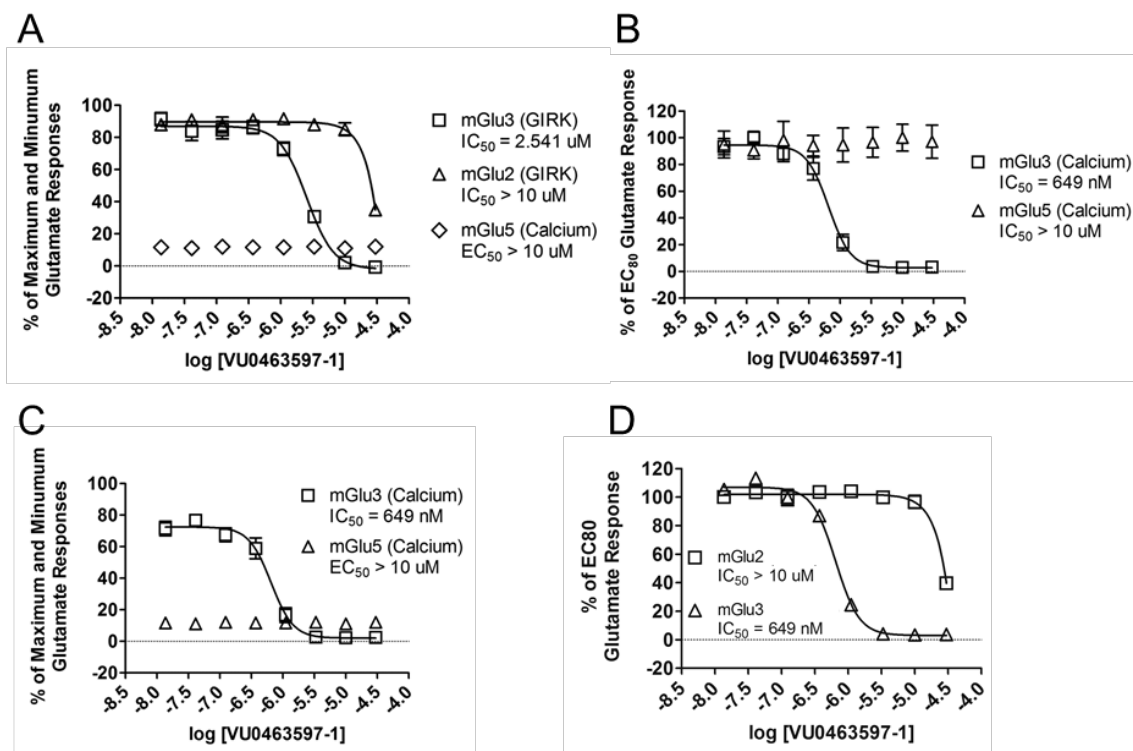


**Figure 3.** In vitro molecular pharmacology characterization of **12** (VU0463597). (A) Concentration-response curves of mGlu<sub>2</sub> and mGlu<sub>3</sub> GIRK (antagonist mode) and mGlu<sub>5</sub> calcium (PAM mode). (B) mGlu<sub>3</sub> calcium (antagonist mode) and mGlu<sub>5</sub> calcium (antagonist mode). (C) mGlu<sub>3</sub> calcium (antagonist mode) and mGlu<sub>5</sub> calcium (PAM mode). (D) mGlu<sub>3</sub> calcium selectivity versus mGlu<sub>2</sub> (antagonist mode).

With a potent and selective mGlu<sub>3</sub> NAM, we began profiling **19** in a battery of ancillary pharmacology and DMPK assays to assess the quality of this probe for potential *in vivo* studies. A Lead Profiling Screen at Ricerca<sup>41</sup> (68 GPCRs, ion channels and transporters screened at 10  $\mu M$  in radioligand binding assays) failed to identify any off target activities for **19** (no inhibition >25% @ 10  $\mu M$ ). In our tier 1 in vitro DMPK assays, **19** had a very clean CYP profile (>30  $\mu M$  vs. CYPs 3A4, 2C9, 2D6 and 1A2), had plasma free fractions of ~1% in rat and 2% in human with a  $f_u$  in rat brain of ~1%. Intrinsic clearance experiments in both rat and human microsomes suggested that **19** would be a rapidly cleared compound (rat:  $t_{1/2} = 11.6$  min,  $CL_{int} = 240$  mL/min/kg,  $CL_{hep}$

= 54.2 mL/min./kg; human:  $t_{1/2}$  = 2.18 min,  $CL_{int}$  = 571.8 mL/min/kg,  $CL_{hep}$  = 20.3 mL/min./kg). To determine if the *in vitro* experiment accurately predicted *in vivo* disposition, we performed rat IV PK (1 mg/kg) and found **19** to be a moderately cleared compound ( $CL$  = 32.9 mL/min/kg) but with a short half-life ( $t_{1/2}$  = 16.8 min) and low volume of distribution ( $V_D$  = 0.6 L/kg). Metabolite ID studies in rat microsomes shed light on the disposition profile of **19** (**Figure 3**). The major route of metabolism was a CYP-mediated O-demethylation of **19** to generate the free phenol **21**. In order to test the activity of the free phenol **21**, O-demethylation of **19** was carried out in the presence of  $BBR_3$  (**Scheme 3**). Upon being screened in the mGlu<sub>3</sub> GIRK channel thallium flux assay, this derivative was found to be inactive.

As our earlier SAR work indicated, the methyl ether was critical for mGlu<sub>3</sub> NAM activity. Therefore, we performed an IP plasma:brain level (PBL) study to determine if we could achieve meaningful CNS exposure if we bypassed first-pass metabolism. Significantly, in a 10 mg/kg (10% Tween80 in 0.5% methylcellulose) IP plasma:brain level (PBL) study, we observed a  $Brain_{AUC}(16.3 \text{ mM}):Plasma_{AUC}(9.7 \text{ mM})$  of 1.67, indicating that **19** (VU0463597) was indeed centrally penetrant. Based on brain homogenate binding studies, this correlates to ~163 nM free drug in rat brain at a 10 mg/kg IV dose, a value below the mGlu<sub>3</sub>  $IC_{50}$  (649 nM). Therefore, a 50 mg/kg dose may be required for *in vivo* efficacy with this first generation mGlu<sub>3</sub> NAM probe.

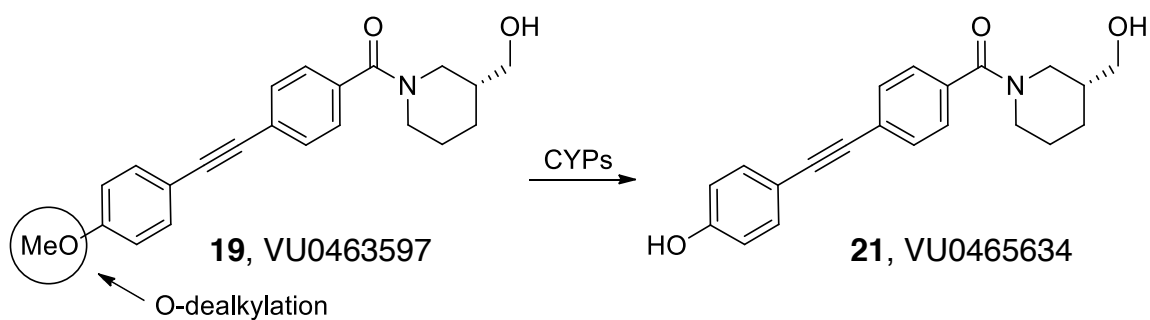
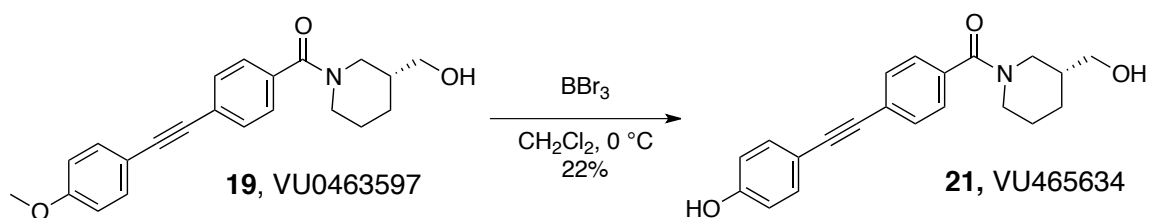
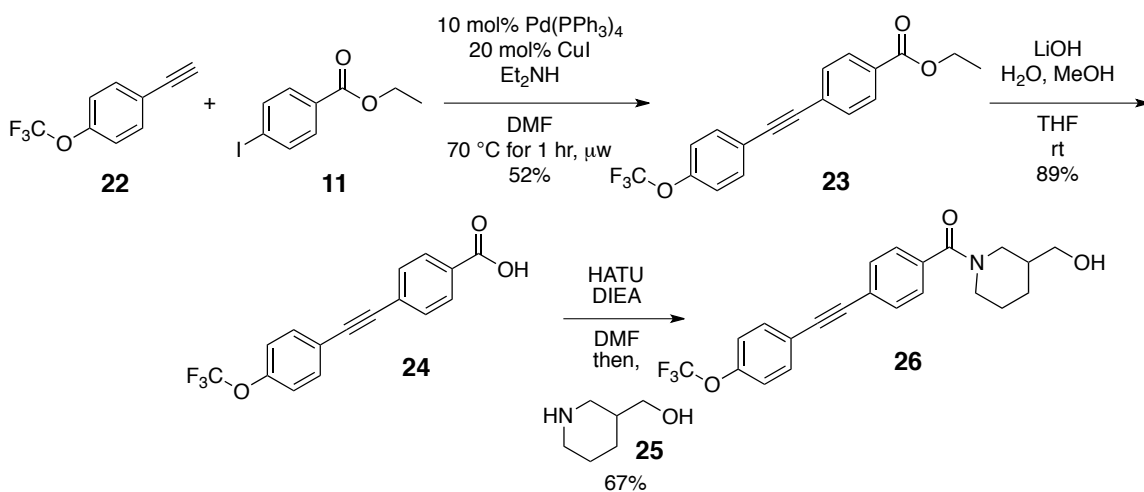


**Figure 4.** Metabolite ID studies in rat microsomes showed the major metabolite of **19** is phenol **21**, via O-dealkylation of the methyl ether.



**Scheme 3.** Synthesis of O-demethylation product **21**

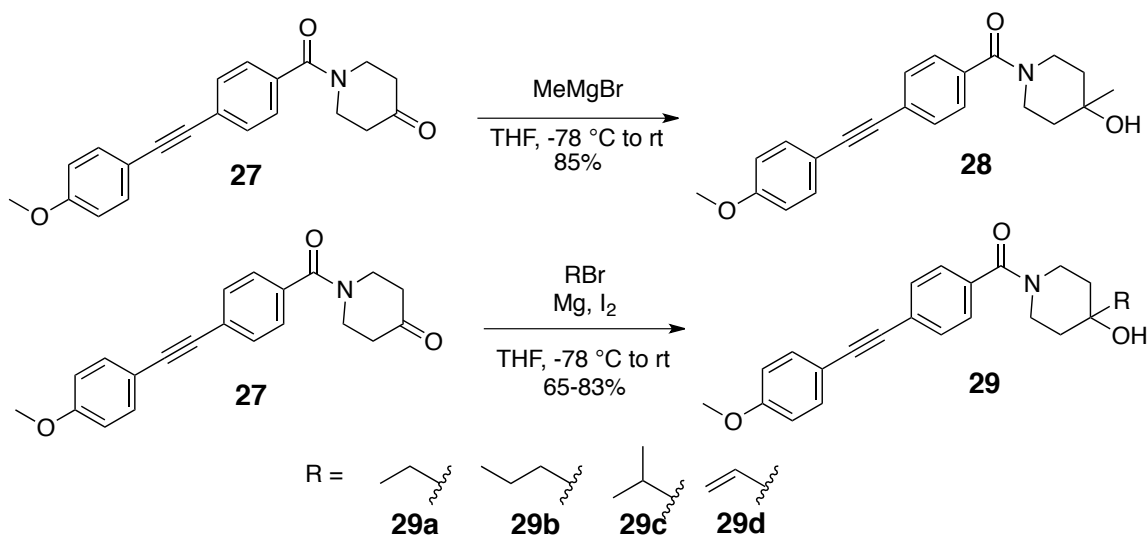
In an effort to avoid the *O*-demethylation, it was desired to synthesize the trifluoromethyl ether derivative **26** shown in Scheme 4. Preliminary DMPK data has shown that the trifluoromethyl functionality prevents dealkylation, however **26** is inactive as a mGlu<sub>3</sub> antagonist.



**Scheme 4.** Synthesis of trifluoromethyl ether analog **26**

### 3.4 Analog development using Grignard additions

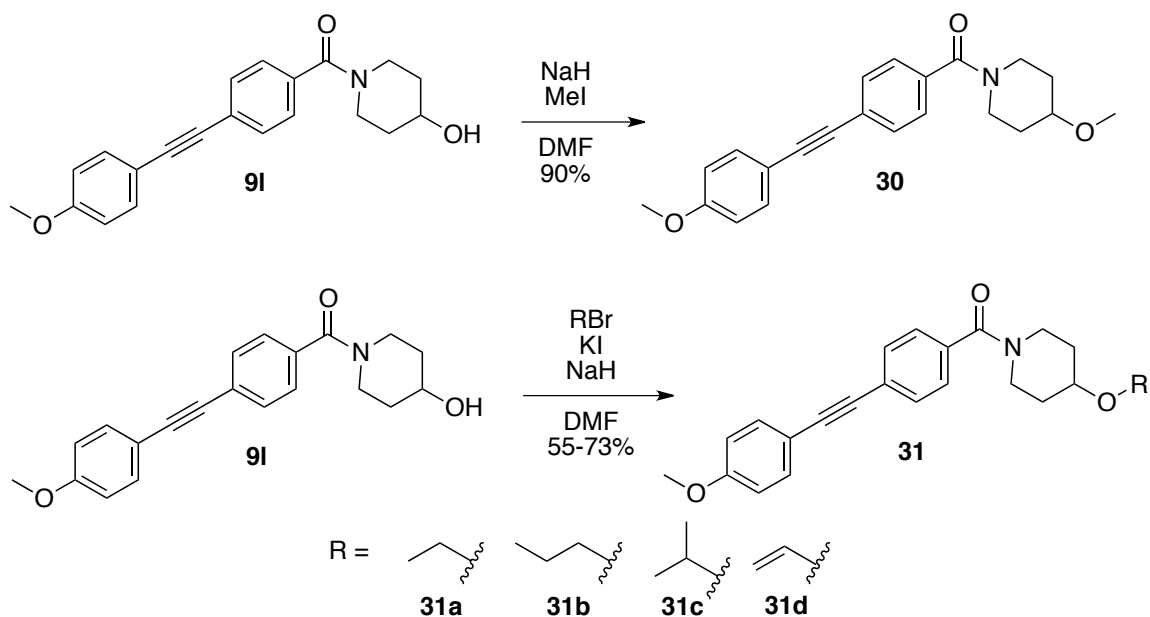
In an effort to further explore SAR around the eastern portion of the molecule several different strategies were utilized. First, using a Grignard addition strategy shown in Scheme 5, we were able to arrive at a variety of tertiary alcohols based on the structure of VU0092273 (**5**). Methyl (**28**) and ethyl (**29a**) Grignard addition products were screened and showed modest mGlu<sub>3</sub> antagonist activity. The bulkier Grignard addition products were inactive (i.e. **22e**).



**Scheme 5.** Synthesis of Grignard products **28-29d**

### 3.5 Analog development via *O*-alkylation of VU0092273

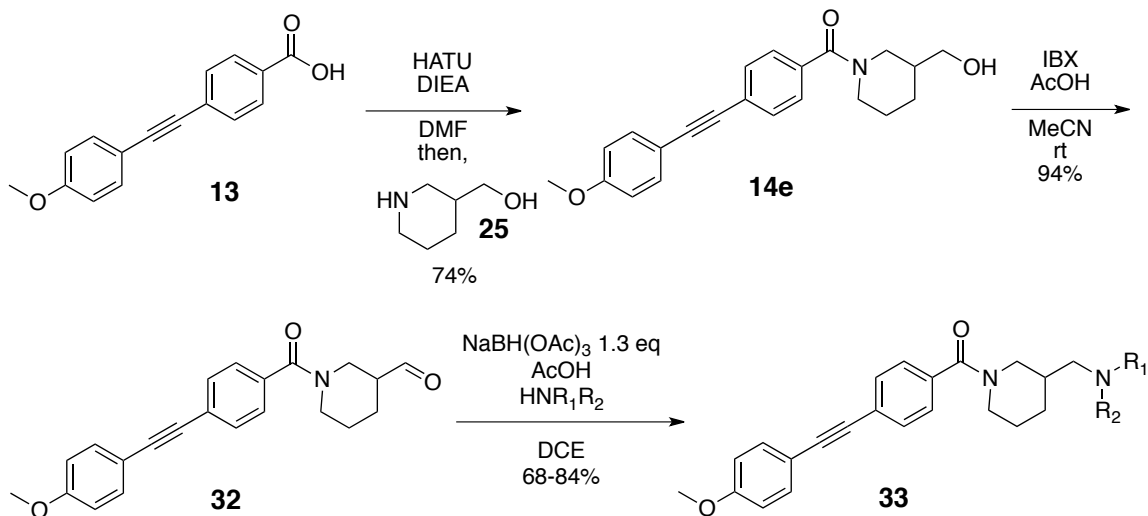
In keeping with the strategy of maintaining structural similarities to VU0092273 (**5**), the next series of reactions examined was the *O*-alkylation of **5**. *O*-alkylation was achieved via sodium hydride deprotonation of the scaffold in DMF followed by addition of the alkyl iodide that was either commercially available or synthesized *in situ* via Finklestein conditions (**Scheme 6**). Yields and time of reaction were acceptable when methyl iodide and allyl iodide were the reacting alkyl halides. However, the alkyl bromides under Finklestein conditions required excess of potassium iodide and alkyl bromide, and reaction times were at least 16 hours. None of these derivatives were active as mGlu<sub>3</sub> antagonists.



**Scheme 6.** Synthesis of *O*-alkylation analogs **30-31d**

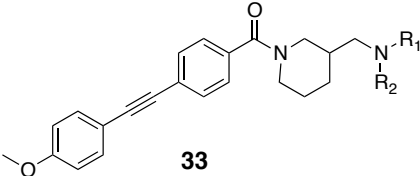
### 3.6 Analog development via reductive aminations

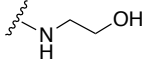
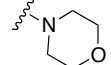
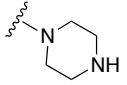
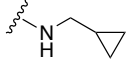
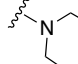
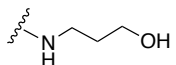
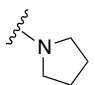
The final 23-membered library explored derivatives that do not involve changes to the basic diphenylacetylene scaffold. These analogs were obtained via  $\text{NaBH}(\text{OAc})_3$  mediated reductive aminations onto aldehyde **32**, which was obtained by IBX oxidation of **14e** (Scheme 7). Interestingly, 22 of the 23 analogs showed at minimum weak antagonist activity at  $\text{mGlu}_3$ , however this was without selectivity over  $\text{mGlu}_2$  (Table 2). It will be of future interest to explore other amines in this reaction in order to improve activity as  $\text{mGlu}_3$  antagonists while dialing out activity at  $\text{mGlu}_2$ .



**Scheme 7.** Synthesis of generic amine **33** via reductive amination

**Table 2.** Representative reductive amination products **33** and activities at mGlu<sub>2</sub> and mGlu<sub>3</sub>



Cmpd	NR <sub>1</sub> R <sub>2</sub>	mGlu <sub>3</sub> IC <sub>50</sub> (μM)	%Glu <sub>3</sub> min	mGlu <sub>2</sub> IC <sub>50</sub> (μM)	%Glu <sub>2</sub> min
<b>33a</b>		2.32	-9.27	>10	12.46
<b>33b</b>		>10	4.68	>10	-1.70
<b>33c</b>		4.39	10.25	2.99	3.29
<b>33d</b>		2.54	8.94	1.92	6.38
<b>33e</b>		3.43	1.35	2.54	-1.55
<b>33f</b>		3.45	18.40	3.09	10.05
<b>33g</b>		4.07	10.26	2.30	5.72



### 3.7 Chapter summary

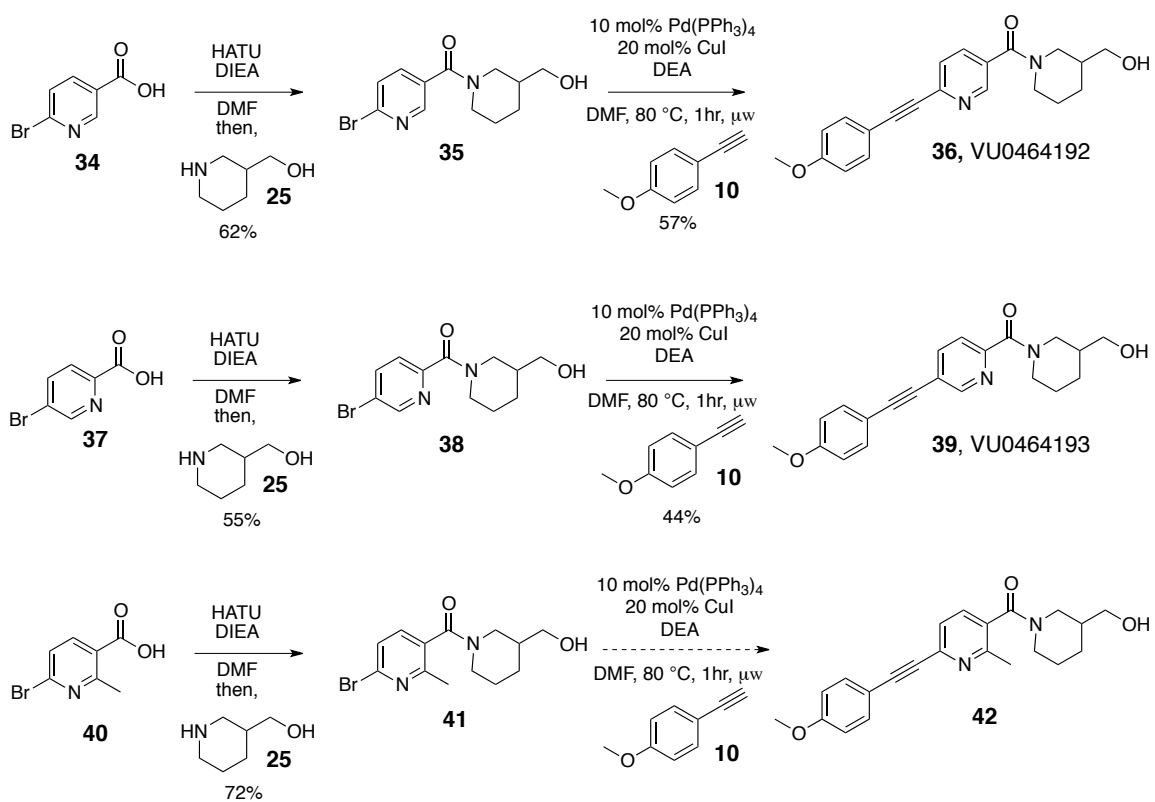
In summary, mGlu<sub>3</sub> NAM activity of the *p*-OMePh scaffold has been improved greater than 2-fold by optimizing the eastern region of the lead compound so that the new lead is the 3-hydroxymethyl analog **14e**. Resolution of the racemic 3-hydroxymethyl analog led us to find that the (*R*)-enantiomer **19** was about 2-fold more potent than the (*S*)-enantiomer **20** in the mGlu<sub>3</sub> GIRK assay. Further pharmacological characterization showed that the major metabolite of VU0463597 was the *O*-dealkylation product of the methyl ether to form **21**. This *O*-dealkylation product was inactive in the mGlu<sub>3</sub> GIRK assay; however, the metabolite profile provides guidance for the syntheses of new analogs that are necessary before *in vivo* studies commence.

## CHAPTER IV

### CURRENT EFFORTS AND FUTURE DIRECTIONS

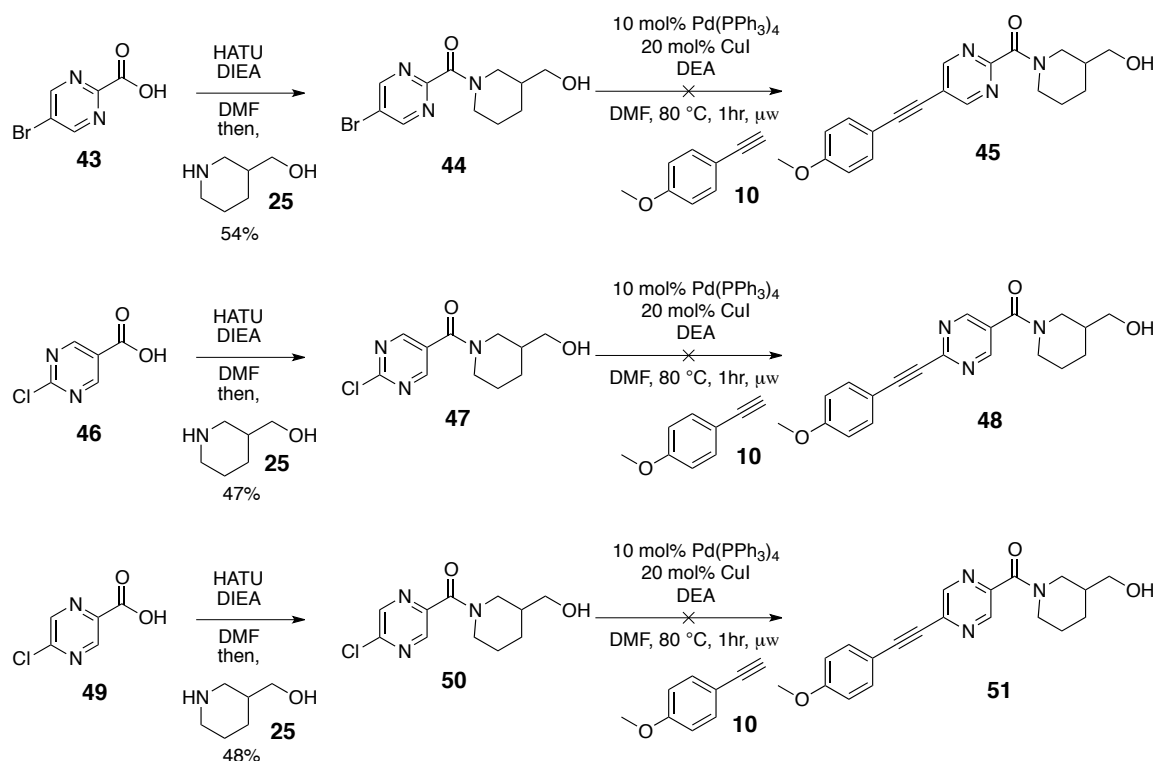
#### 4.1 Current efforts utilizing molecular switches

In effort to continue improving the potency and selectivity of our mGlu<sub>3</sub> negative allosteric modulator (NAM) lead compound and possibly finding other modes of pharmacology, we are investigating the use of subtle molecular switches within the diphenylacetylene scaffold. By modifying the phenyl groups of the diphenylacetylene scaffold with nitrogen heterocycles we seek to access a scaffold with improved potency and pharmacokinetics. To this point, these efforts have included substituting the proximal phenyl ring with pyridinyl moieties to access compounds shown in Scheme 1. Upon testing the activity of these compounds in the GIRK assay, these derivatives were found to be inactive at both mGlu<sub>3</sub> and mGlu<sub>2</sub>.

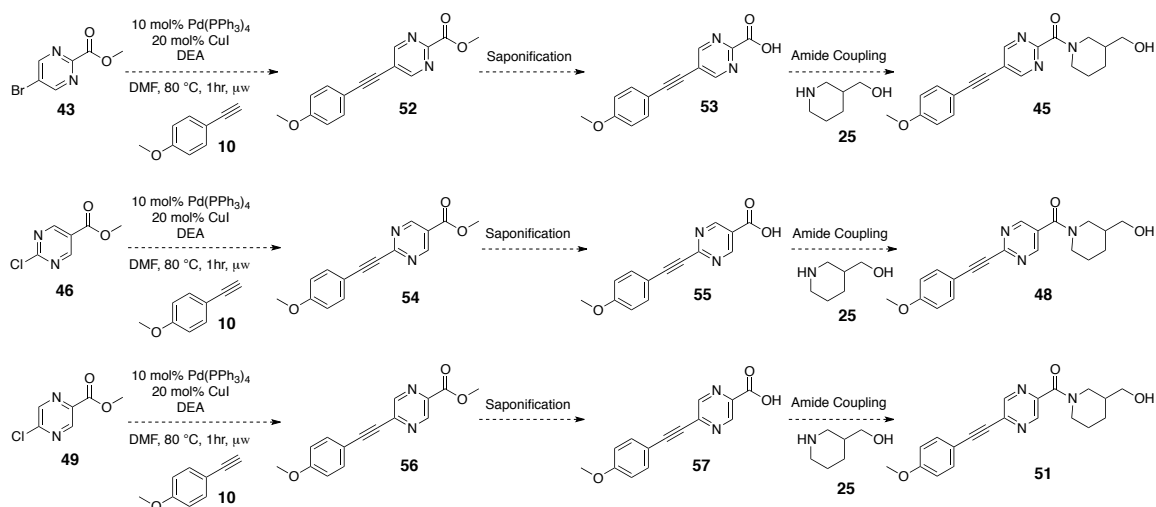


**Scheme 1.** Synthesis of pyridinyl analogs VU0464192 (**36**), VU04964193 (**39**), and **42** from brominated nicotinic and picolinic acid derivatives

We have also worked to synthesize derivatives containing pyrazine, pyrimidine, and pyridazine moieties within the proximal aromatic ring (**Scheme 2**). Amides **44**, **47**, and **50** are readily obtainable via HATU mediated amide coupling reactions, however, upon utilizing Sonagashira coupling conditions to couple 4-ethynyl anisole **10**, no appreciable products were recovered. It will be advantageous to attempt arriving at these desired products via the Sonagashira coupling of **10** with the esters of **43**, **46**, and **49** (**Scheme 3**).



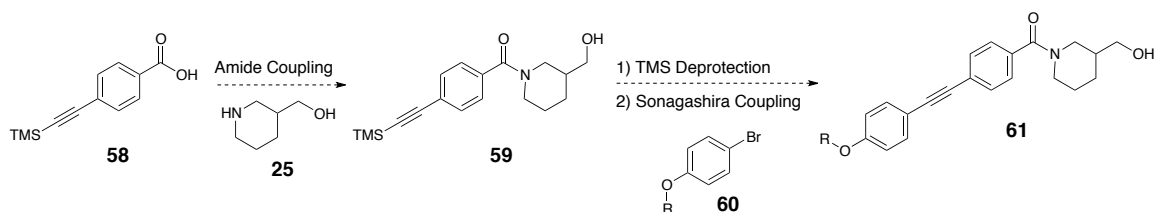
**Scheme 2.** Synthesis of pyrimidines **45** and **48** and pyrazine **51**



**Scheme 3.** Alternative route to arrive at pyrimidines **45** and **48** and pyrazine **51**

#### 4.2 Future efforts aimed at improving pharmacokinetics of mGlu<sub>3</sub> probe

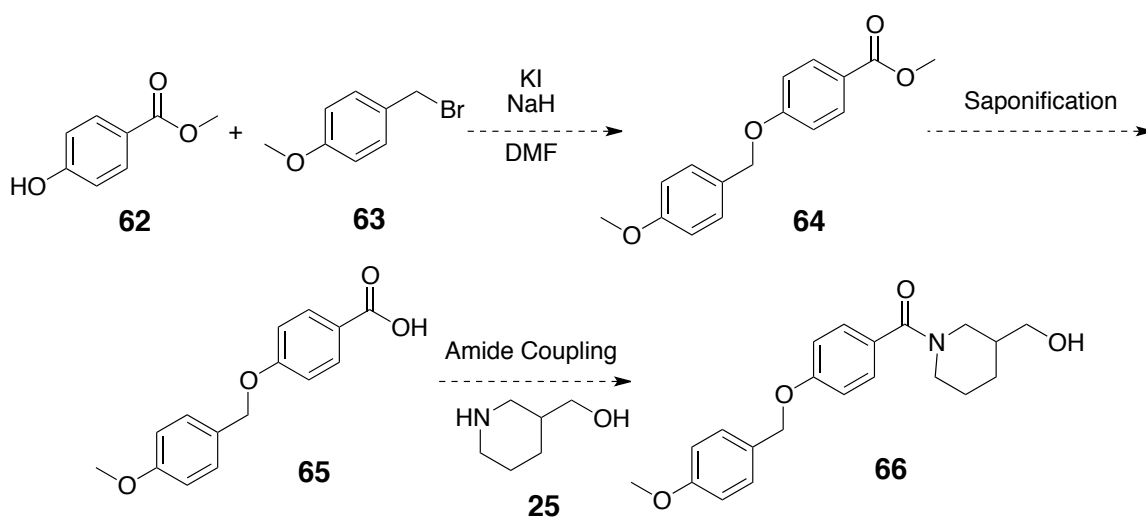
With a potent and selective mGlu<sub>3</sub> NAM in hand (**19**), it will be advantageous to discover a probe with improved *in vivo* properties. Since the primary metabolism pathway of **19** is dealkylation of the methoxy ether it will be necessary to install functionality that prevents this CYP mediated dealkylation. As discussed in Chapter 3, the first effort at approaching this issue was to substitute the methyl ether of **19** with trifluoromethyl ether **26**. Since **26** was inactive as an mGlu<sub>3</sub> NAM, the next strategy will be to incorporate substituted alkyl ethers (**Scheme 4**). Starting with commercially



**Scheme 4.** Proposed route to generic substituted alkyl ether **61**

available TMS acetylene **58** it is proposed that we could arrive at **61** via an amide coupling with **25** to provide amide **59** followed by TMS deprotection and a Sonagashira coupling with a range of *p*-brominated aryl ethers (**60**) to furnish **61**.

It has been postulated that mGlu allosteric modulators of the MPEP-chemotype are not suitable for therapeutic development due to the metabolic and toxicologic liability constituted by the potentially reactive acetylene linker.<sup>42</sup> As a consequence, it is desirable to remove the acetylenic linker while designing analogs that maintain the relative geometry of the two aryl rings. Recent studies toward developing mGlu<sub>5</sub> positive allosteric modulators (PAMs) in our group have shown that the acetylenic linker can be replaced by a benzyl ether and maintain activity. An effort is currently underway to investigate the applicability of this strategy to mGlu<sub>3</sub> NAMs (Scheme 5). Beginning with commercially available methyl ester **62** and benzyl bromide **63**, benzyl ether **64** could be obtained under Finklestein conditions. Saponification of the methyl ester of **64**, followed by the coupling of amine **25** with acid **65** one could arrive at benzyl ether **66**.



**Scheme 5.** Route to obtain benzyl ether **66**

### 4.3 Chapter summary

Utilizing our knowledge of the molecular switch phenomenon in regard to mGlu<sub>3</sub> allosteric modulation, we aim at improving the activity, potency, and pharmacokinetics of our current mGlu<sub>3</sub> NAM lead **19**. Modifying the diphenylacetylene scaffold by incorporating nitrogen heterocycles has, thus far, not yielded any active mGlu<sub>3</sub> NAMs. Future efforts will be aimed at reducing the rate of metabolism of our lead compound **19** so that we can conduct further *in vivo* studies regarding the selective modulation of mGlu<sub>3</sub>. The strategies for reducing CYP metabolism are currently aimed at substituting the methyl ether and acetylene moieties of **19**. Reduced metabolism and mGlu<sub>3</sub> NAM activity preservation could potentially be achieved by substituting the methyl ether and acetylene with a branched alkyl group and benzyl ether moiety respectively.

From this work, we have reported the first selective mGlu<sub>3</sub> NAM. However, it is necessary to improve the therapeutic value of these modulators through further modifications. Ultimately, developing a more potent and bioavailable mGlu<sub>3</sub> negative allosteric modulator will allow us to gain a better understanding of mGlu<sub>3</sub> function in the pathogenesis of CNS disorders.

## CHAPTER 5

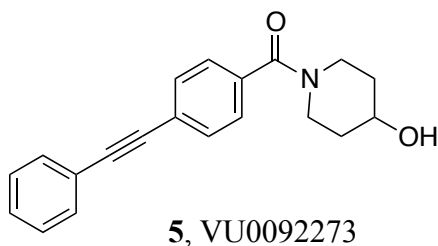
### EXPERIMENTAL

#### 5.1 Methods and Materials

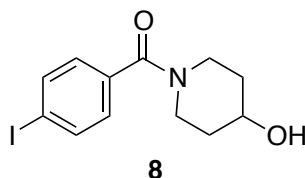
**General experimental.** All NMR spectra were recorded on a Bruker 400 MHz instrument.  $^1\text{H}$  chemical shifts are reported in  $\delta$  values in ppm downfield from DMSO as the internal standard in DMSO. Data are reported as follows: chemical shift, multiplicity (s = singlet, d = doublet, t = triplet, q = quartet, br = broad, m = multiplet), integration, coupling constant (Hz).  $^{13}\text{C}$  chemical shifts are reported in  $\delta$  values in ppm with the DMSO carbon peak set to 39.5 ppm. Low resolution mass spectra were obtained on an agilent 1200 series 6130 mass spectrometer. High resolution mass spectra were recorded on a Waters Q-TOF API-US. Analytical HPLC was performed on an Agilent 1200 series. Preparative purification was performed on combi-flash companion. Solvents for extraction, washing and chromatography were HPLC grade.



**Standard experimental procedures for key compounds:**

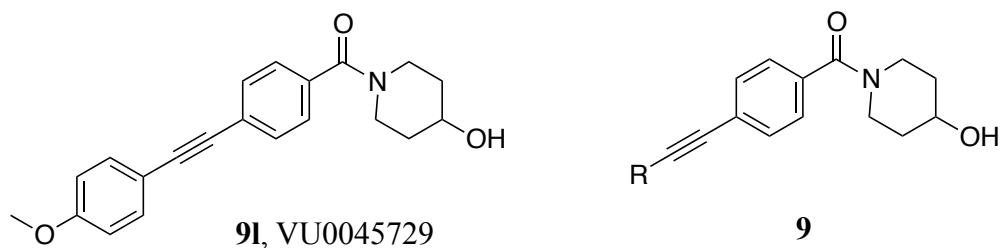


**(4-hydroxypiperidin-1-yl)(4-phenylethynyl)phenylmethanone, VU0092273 (5).** To a solution of acid **9** (1.40 g, 6.30 mmol) and DIPEA (2.70 g, 20.8 mmol) in DMF (25 mL) was added EDC (1.41 g, 7.56 mmol), HOBt (850 mg, 6.30 mmol) and 4-hydroxypiperidine hydrochloride (1.29 g, 9.46 mmol). The reaction was stirred at room temperature for 18 h. The reaction was diluted with water (100 mL) and isolated amide **3a** (1.84 g, 98%) as a white solid by vacuum filtration: mp 157.7 °C; <sup>1</sup>H-NMR (400 MHz, CDCl<sub>3</sub>) δ 7.58 (d, *J* = 8.0 Hz, 2H), 7.56-7.52 (m, 2H), 7.44-7.34 (m, 5H), 4.21-4.08 (m, 1H), 4.03-3.96 (m, 1H), 3.81-3.48 (m, 1H), 3.47-3.16 (m, 2H), 2.08-1.79 (m, 3H), 1.71-1.42 (m, 2H); <sup>13</sup>C-NMR (100 MHz, CDCl<sub>3</sub>) δ 169.7, 135.5, 131.6, 131.5, 128.5, 128.3, 126.9, 124.7, 122.8, 90.8, 88.5, 66.9, 44.8, 39.3, 34.4, 33.8; LC (214 nm) 2.86 min (>98%); MS (ESI) *m/z* = 306.1; HRMS = 306.1496 (calc. 306.1494), C<sub>20</sub>H<sub>20</sub>N<sub>1</sub>O<sub>2</sub>.

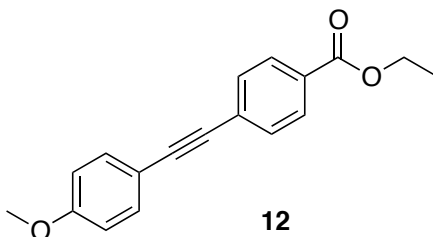


**(4-hydroxypiperidin-1-yl)(4-iodophenyl)methanone, (8).** To a solution of acid **6** (1.56 g, 6.30 mmol) and DIPEA (2.70 g, 20.8 mmol) in DMF (25 mL) was added EDC (1.41 g,

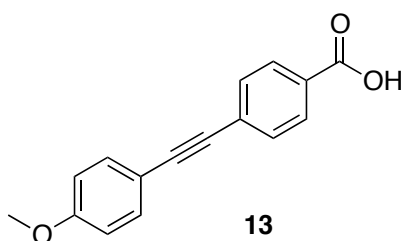
7.56 mmol), HOBt (850 mg, 6.30 mmol) and 4-hydroxypiperidine hydrochloride (1.29 g, 9.46 mmol). The reaction was stirred at room temperature for 18 h. The reaction was diluted with water (100 mL) and the organic phase was dried over MgSO<sub>4</sub>, filtered and concentrated under vacuum. The crude product was purified by column chromatography (silica gel) using 0 to 10 % MeOH/EtOAc to afford amide **8** (1.67 g, 80%).



**Representative experimental for the synthesis of (4-hydroxypiperidin-1-yl)(4-((4-methoxyphenyl)ethynyl)phenyl)methanone (91) and functionalized acetylene analogs (9).** To a solution of (4-hydroxypiperidin-1-yl)(4-iodophenyl)methanone **8** (20 mg, 0.06 mmol) in DMF (0.54 mL) was added 4-ethynyl anisole **10** (9.90 mg, 0.075 mmol), Pd(Ph<sub>3</sub>P)<sub>4</sub> (2.3 mg, 0.002 mmol), CuI (0.5 mg, 0.003 mmol) and diethylamine (7.2 μL). The reaction vessel was sealed and heated at 60 °C for 1h in a microwave reactor. The reaction was cooled to rt, diluted with EtOAc:hexanes (2:1, 3 mL) and washed with water (2 x 5 mL) and brine (5 mL). The organic phase was dried over MgSO<sub>4</sub>, filtered and concentrated under vacuum. The crude product was purified by preparative HPLC to afford **91**.

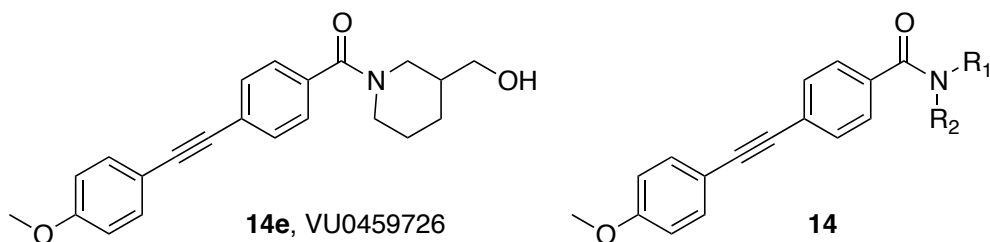


**Ethyl 4-(phenylethynyl)benzoate (12).** To a solution of ethyl 4-Iodobenzoate **11** (5.0 g, 18.2 mmol) in DMF (8 mL) was added 4-ethynyl anisole **10** (2.25 g, 22.1 mmol), Pd(Ph<sub>3</sub>P)<sub>4</sub> (502 mg, 0.45 mmol), CuI (172 mg, 0.91 mmol) and diethylamine (2 mL). The reaction vessel was sealed and heated at 60 °C for 1h in a microwave reactor. The reaction was cooled to rt, diluted with EtOAc:hexanes (2:1, 150 mL) and washed with water (2 x 100 mL) and brine (100 mL). The organic phase was dried over MgSO<sub>4</sub>, filtered and concentrated under vacuum. The crude product was purified by column chromatography (silica gel) using 0 to 10 % EtOAc/hexanes to afford ester **2** (7.89 g, 86%) as a pale yellow solid: <sup>1</sup>H-NMR (400 MHz, CDCl<sub>3</sub>) δ 8.05 (d, *J* = 8.0 Hz, 2H), 7.61 (d, *J* = 8.0 Hz, 2H), 7.56 (dd, *J* = 8.0, 2.0 Hz, 2H), 7.41-7.37 (m, 3H), 4.41 (q, *J* = 7.0 Hz, 2H), 1.44 (t, *J* = 7.0 Hz, 3H); LC (214 nm) 5.79 min (>98%); MS (ESI) *m/z* = 250.9.



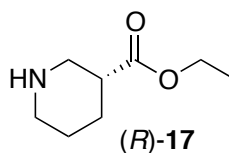
**4-(phenylethynyl)benzoic acid (13).** To a solution of ester **12** (7.81 g, 31.2 mmol) in THF (80 mL) was added MeOH (15 mL) and a solution of LiOH (5.24 g, 124 mmol) in water (15 mL). The reaction was stirred at room temperature and for 4h. The reaction was

acidified with 1 N HCl (50 mL) and isolated benzoic acid (5.78 g, 83%) as a white solid: mp 190.1 °C; <sup>1</sup>H-NMR (400 MHz, CDCl<sub>3</sub>) δ 8.11 (d, *J* = 8.0 Hz, 2H), 7.64 (d, *J* = 8.0 Hz, 2H), 7.62-7.56 (m, 2H), 7.52-7.47 (m, 1H), 7.43-7.36 (m, 3H); <sup>13</sup>C-NMR (100 MHz, *d*<sub>6</sub>-DMSO) δ 167.3, 138.0, 134.5, 131.9, 131.4, 130.9, 130.6, 130.2, 130.0, 129.6, 127.0, 122.15, 101.6, 92.3, 89.0; LC (214 nm) 5.12 min (>98%); MS (ESI) *m/z* = 222.9.

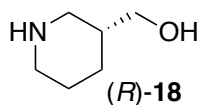


**Representative experimental for the synthesis of (3-(hydroxymethyl)piperidin-1-yl)(4-((4-methoxyphenyl)ethynyl)phenyl)methanone (14e) and amide analogs (14).**

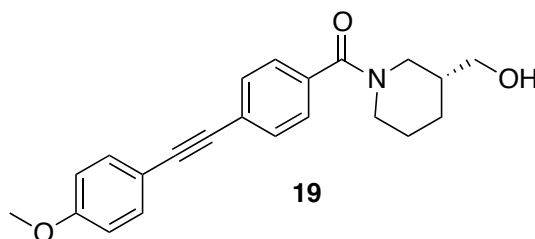
To a solution of acid **13** (30 mg, 0.12 mmol) and DIPEA (0.1 mL, 0.6 mmol) in DMF (0.3 mL) was added HATU (45.6 mg, 0.12 mmol). The reaction was stirred for 20 min at rt, then 3-(hydroxymethyl)piperidine (15.0 mg, 0.13 mmol) was added. The reaction was stirred at room temperature for 18 h. The reaction was diluted with water (2 mL) and the organic was dried over MgSO<sub>4</sub>, filtered and concentrated under vacuum. The crude product was purified by preparative HPLC to afford **14e**.



**(R)-ethyl piperidine-3-carboxylate ((R)-17).** To a suspension of acid *(R)*-16 (100 mg, 0.775 mmol) in EtOH (10 mL) was added concentrated sulfuric acid (33  $\mu$ L). The mixture was heated to reflux for 24 h. The reaction was concentrated *in vacuo* and the residue was brought to pH 8 with saturated sodium bicarbonate. The mixture was extracted with EtOAc (3 x 10 mL). The organic extracts were combined and washed with brine (5 mL). The organic phase was dried over MgSO<sub>4</sub>, filtered, and concentrated under vacuum. The residue *(R)*-17 was carried to the next step without purification.

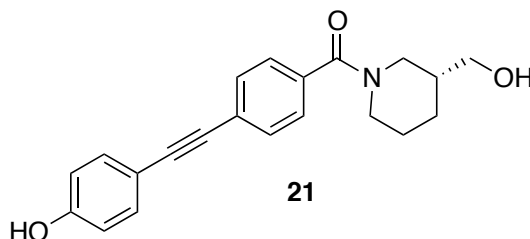


**(R)-3-(hydroxymethyl)piperidine ((R)-18).** To a solution of LAH (14.4 mg, 0.39 mmol) in THF (0.5 mL) at 0 °C flashed with argon was added *R*-17 (30 mg, 0.19 mmol) as a solution in THF (0.5 mL). THF (0.5 mL) was added, and the reaction was heated to reflux under argon for 4 h. The reaction was quenched by adding saturated sodium sulfate dropwise. The mixture was filtered and washed with diethyl ether. The organic phase was dried over Na<sub>2</sub>SO<sub>4</sub>, and concentrated *in vacuo* to afford *R*-18 (82.5% over 2 steps).



**(*R*)-3-(hydroxymethyl)piperidin-1-yl(4-((4-methoxyphenyl)ethynyl)phenyl)**

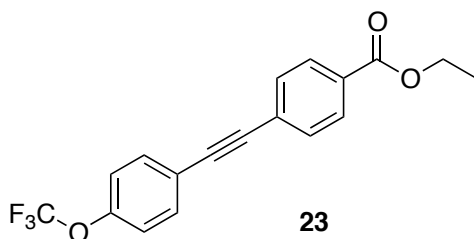
**methanone (19).** To a solution of acid **6** (30 mg, 0.12 mmol) and DIPEA (0.1 mL, 0.6 mmol) in DMF (0.3 mL) was added HATU (45.6 mg, 0.12 mmol). The reaction was stirred for 20 min at rt, then (*R*)-**18** (15.0 mg, 0.13 mmol). The reaction was stirred at room temperature for 18 h. The reaction was diluted with water (2 mL) and the organic was dried over MgSO<sub>4</sub>, filtered and concentrated under vacuum. The crude product was purified by preparative HPLC to afford **19**.



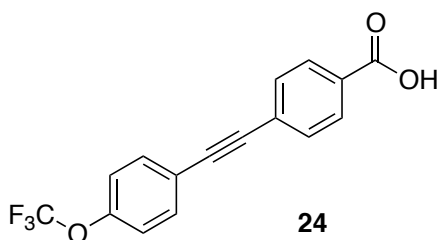
**(*R*)-3-(hydroxymethyl)piperidin-1-yl(4-((4-hydroxyphenyl)ethynyl)phenyl)**

**methanone (21).** To a solution of **19** (20 mg, 0.057 mmol) in CH<sub>2</sub>Cl<sub>2</sub> (0.5 mL) cooled to 0 °C and flashed with argon was added BBr<sub>3</sub> (21.65 μL, 0.229 mmol) dropwise. The reaction was allowed to warm to room temperature and stirred for 4h. The reaction was diluted with DCM (2mL) and then washed sequentially with 1M HCl (0.5 mL), saturated aq. NaHCO<sub>3</sub> (1 mL) and 1N NaOH (1 ml). The organic layer was dried over Na<sub>2</sub>SO<sub>4</sub>,

filtered and concentrated under vacuum. The crude product was purified by preparative HPLC to afford **21** (4.2 mg, 22%).

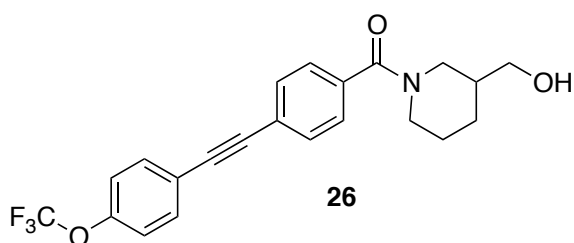


**Ethyl 4-((4-(trifluoromethoxy)phenyl)ethynyl)benzoate (23).** To a solution of ethyl 4-Iodobenzoate **11** (177.9 mg, 0.645 mmol) in DMF (3 mL) was added 1-ethynyl-4-(trifluoromethoxy)benzene **22** (82.3  $\mu$ L, 0.537 mmol), Pd(PH<sub>3</sub>P)<sub>4</sub> (62.4 mg, 0.054 mmol), CuI (10.3 mg, 0.054 mmol) and diethylamine (61.1  $\mu$ L, 0.591 mmol). The reaction vessel was sealed and heated at 60 °C for 1h in a microwave reactor. The reaction was cooled to rt, diluted with EtOAc:hexanes (2:1, 3 mL) and washed with water (2 x 2 mL) and brine (2 mL). The organic phase was dried over MgSO<sub>4</sub>, filtered and concentrated under vacuum. The crude product was purified by column chromatography (silica gel) using 0 to 5 % EtOAc/hexanes to afford ester **26**.

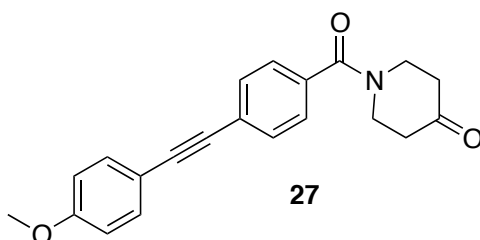


**4-((4-(trifluoromethoxy)phenyl)ethynyl)benzoic acid (24).** To a solution of ester **23** (179.51 mg, 0.537 mmol) in THF (2 mL) was added MeOH (0.5 mL) and a solution of

LiOH (51.44 g, 2.148 mmol) in water (0.5 mL). The reaction was stirred at room temperature and for 4h. The reaction was acidified with 1 N HCl (50 mL) and isolated benzoic acid **24**.



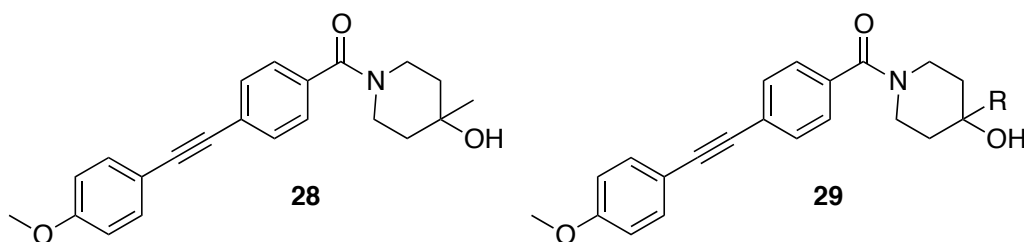
**(3-(hydroxymethyl)piperidin-1-yl)(4-((4-(trifluoromethoxy)phenyl)ethynyl)phenyl)methanone (26)**. To a solution of acid **24** (25 mg, 0.082 mmol) and DIPEA (45  $\mu$ L, 0.245 mmol) in DMF (0.3 mL) was added HATU (31.06 mg, 0.082 mmol). The reaction was stirred for 20 min at rt, then 3-(hydroxymethyl)piperidine (15.0 mg, 0.13 mmol). The reaction was stirred at room temperature for 18 h. The reaction was diluted with water (2 mL) and the organic was dried over  $MgSO_4$ , filtered and concentrated under vacuum. The crude product was purified by preparative HPLC to afford **26**.



**1-(4-((4-methoxyphenyl)ethynyl)benzoyl)piperidin-4-one (27)**. To a solution of acid **13** (100 mg, 0.4 mmol) and DIPEA (0.2 mL, 1.2 mmol) in DMF (1.0 mL) was added HATU (167.2 mg, 0.44 mmol). The reaction was stirred for 20 min at rt, then 4-

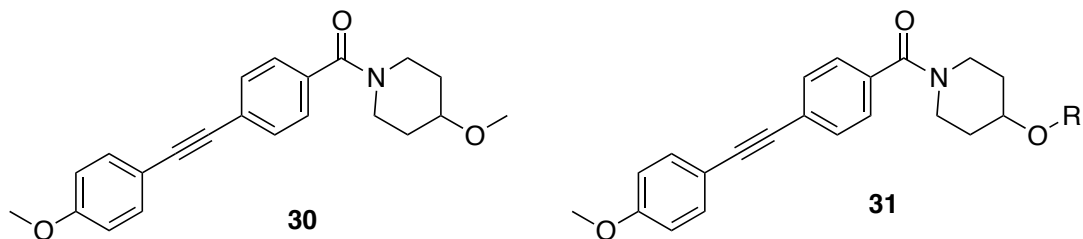


piperidinone (43.67 mg, 0.44 mmol). The reaction was stirred at room temperature for 18 h. The reaction was diluted with water (5 mL) and the organic was dried over MgSO<sub>4</sub>, filtered and concentrated under vacuum. The crude product was purified by column chromatography (silica gel) using 0 to 5 % EtOAc/hexanes to afford amide **27** (121 mg, 91%) as a white solid.

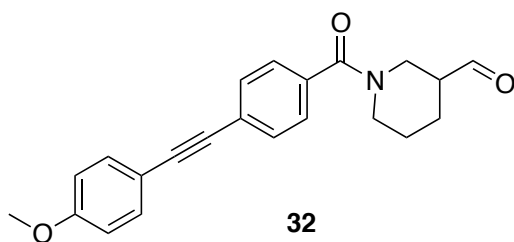


**Representative experimental for the synthesis of (3-(hydroxymethyl)piperidin-1-yl)(4-((4-methoxyphenyl)ethynyl)phenyl)methanone (28) and amide analogs (29).**

To a solution of methyl magnesium bromide (47  $\mu$ L, 1.4 M in diethyl ether) cooled to -78 °C and purged with argon was added ketone **27** (20 mg, 0.06 mmol) as a solution in THF (0.5 mL) at -78 °C. The reaction was allowed to warm to rt and stirred for 6 h. The reaction was quenched with saturated NH<sub>4</sub>Cl and extracted with EtOAc (3 x 5 mL). The combined extracts were washed with brine (5 mL), dried over MgSO<sub>4</sub>, filtered, and concentrated under vacuum. The crude product was purified by preparative HPLC to afford **28**.

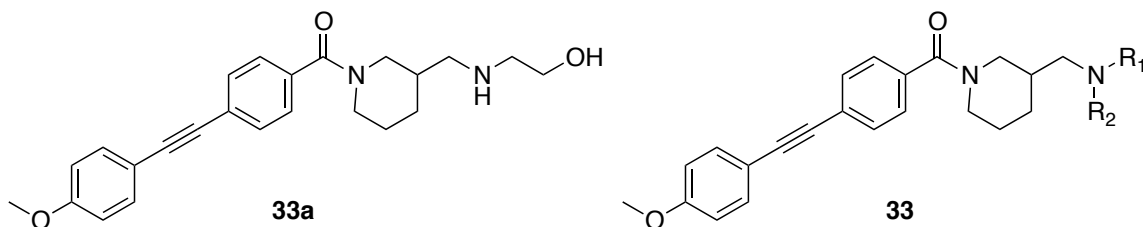


**Representative experimental for the synthesis of (4-((4-methoxyphenyl)ethynyl)phenyl)(4-methoxypiperidin-1-yl)methanone (30) and O-alkylation analogs (31).** To a solution of **5** (25 mg, 0.075 mmol) in DMF (2 mL) at 0 °C was added NaH (2.16 mg). The reactions stirred for 10 min, then methyl iodide (7.03  $\mu$ L, 0.113 mmol) was added dropwise. The reaction was partitioned between water and EtOAc. The organic phase was washed with brine (2 mL), dried over MgSO<sub>4</sub>, filtered and concentrated under vacuum. The crude product was purified by preparative HPLC to afford **30** (23.5 mg, 89.8%) as a white solid.

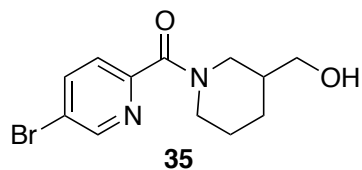


**1-(4-((4-methoxyphenyl)ethynyl)benzoyl)piperidine-3-carbaldehyde (32).** To a solution of **14e** (200 mg, 0.573 mmol) in acetonitrile (3 mL) was added acetic acid (164.3  $\mu$ L, 2.87 mmol) and IBX (1.6 g, 5.8 mmol). The suspension stirred at rt for 4 h. The reaction was quenched by the addition of saturated NaHCO<sub>3</sub>. The crude material was

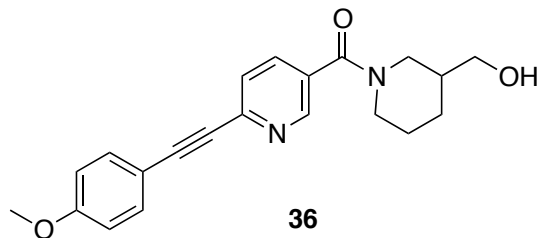
filtered through a pad of silica and concentrated under vacuum to afford **32** (195 mg, 93%).



**Representative experimental for the synthesis of (3-(((2-hydroxyethyl)amino)methyl)piperidin-1-yl)(4-((4-methoxyphenyl)ethynyl)phenyl)methanone (33a) and reductive amination products (33).** To a solution of **32** (8.5 mg, 0.025 mmol) in dichloroethane (0.4 mL) was added ethanolamine (2.22  $\mu\text{L}$ , 0.037 mmol), glacial acetic acid (2.8  $\mu\text{L}$ , 0.049 mmol), and  $\text{NaBH}(\text{OAc})_3$  (6.75 mg, 0.032 mmol). The reaction stirred for 16 h and was quenched by the addition of water (1 mL). The mixture was extracted with EtOAc (3 x 5 mL), and the combined extracts were washed with brine (2 mL) and saturated  $\text{NaHCO}_3$  (2 mL). The organic phase was dried over  $\text{MgSO}_4$ , filtered, and concentrated under vacuum. The crude product was purified by preparative HPLC to afford **33a**.



**Representative experimental for the synthesis of (5-bromopyridin-2-yl)(3-(hydroxymethyl)piperidin-1-yl)methanone (35) and nitrogen heterocycle analogs (38), (41), (44), (47), and (50).** To a solution of acid **34** (50 mg, 0.25 mmol) and DIPEA (0.13 mL, 0.74 mmol) in DMF (1.0 mL) was added HATU (94.3 mg, 0.25 mmol). The reaction was stirred for 20 min at rt, then 3-(hydroxymethyl)piperidine (34.3 mg, 0.30 mmol). The reaction was stirred at room temperature for 18 h. The reaction was diluted with water (5 mL) and the organic was dried over MgSO<sub>4</sub>, filtered and concentrated under vacuum. The crude product was purified by preparative HPLC to afford **35** (18 mg, 24.4%).



**Representative experimental for the synthesis of (3-(hydroxymethyl)piperidin-1-yl)(6-((4-methoxyphenyl)ethynyl)pyridin-3-yl)methanone (36) and nitrogen heterocycle analog 39.** To a solution of **35** (28 mg, 0.134 mmol) in DMF (1 mL) was added 4-ethynyl anisole **10** (20.9  $\mu$ L, 0.161 mmol), Pd(Ph<sub>3</sub>P)<sub>4</sub> (15.5 mg, 0.013 mmol), CuI (2.55 mg, 0.013 mmol) and diethylamine (16.65  $\mu$ L). The reaction vessel was sealed

and heated at 60 °C for 1h in a microwave reactor. The reaction was cooled to rt, diluted with EtOAc:hexanes (2:1, 3 mL) and washed with water (2 x 5 mL) and brine (5 mL). The organic phase was dried over MgSO<sub>4</sub>, filtered and concentrated under vacuum. The crude product was purified by preparative HPLC (basic method) to afford **36** (8.9 mg, 19.0%).

### ***In vitro* profiling**

Human Embryonic Kidney (HEK-293) cell lines co-expressing rat mGlu<sub>3</sub> and G protein inwardly rectifying potassium (GIRK) channels were grown in Growth Media containing 45% DMEM, 45% F-12, 10% FBS, 20 mM HEPES, 2 mM L-glutamine, antibiotic/antimycotic, non-essential amino acids, 700 µg/ml G418, and 0.6 µg/ml puromycin at 37°C in the presence of 5% CO<sub>2</sub>. All cell culture reagents were purchased from Invitrogen Corp. (Carlsbad, CA) unless otherwise noted. Compound activity at the mGlu<sub>3</sub> was assessed using thallium flux through GIRK channels, a method that has been described in detail.<sup>1</sup> Briefly, cells were plated into 384-well, black-walled, clear-bottomed poly-D-lysine-coated plates at a density of 15,000 cells/20 µl/well in DMEM containing 10% dialyzed FBS, 20 mM HEPES, and 100 units/ml penicillin/streptomycin (assay media). Plated cells were incubated overnight at 37°C in the presence of 5% CO<sub>2</sub>. The following day, the medium was exchanged to Assay Buffer [Hanks' balanced salt solution (Invitrogen) containing 20 mM HEPES, pH 7.3] using an ELX405 microplate washer (BioTek), leaving 20 µL/well, followed by addition of 20 µL/well 2X FluoZin-2 AM (330 nM FINAL) indicator dye (Invitrogen, prepared as a DMSO stock and mixed in a 1:1 ratio with pluronic acid F-127) in Assay Buffer, and incubation for 1 h at room

temperature. The dye was then exchanged to Assay Buffer using an ELX405, leaving 20  $\mu\text{L}$ /well. Compounds were serially diluted in assay buffer for a final 2X stock in 0.6% DMSO (0.3% final). A Glutamate EC80 was prepared at a 5X stock solution in Thallium Buffer [125 mM sodium bicarbonate (added fresh the morning of the experiment), 1 mM magnesium sulfate, 1.8 mM calcium sulfate, 5 mM glucose, 12 mM thallium sulfate, and 10 mM HEPES, pH 7.3] prior to addition to assay plates. Thallium flux was measured at 37°C using a kinetic imaging plate reader (FDSS 6000; Hamamatsu Corporation, Bridgewater, NJ) according to the following protocol. Baseline readings were taken (10 images at 1 Hz; excitation,  $470 \pm 20$  nm; emission,  $540 \pm 30$  nm) and test compounds were added in a 20  $\mu\text{L}$  volume and incubated for 144s before the addition of 10  $\mu\text{L}$  of Thallium Buffer with or without an EC80 concentration of Glutamate. Control wells also received a maximal Glutamate concentration (100  $\mu\text{M}$ ) for eventual response normalization. After the addition of agonist, data was collected for an additional 2.5 min and analyzed using Excel (Microsoft Corp, Redmond, WA). The slope of the fluorescence increase beginning 5 s after thallium/agonist addition and ending 15 s after thallium/agonist addition was calculated, corrected to vehicle and maximal Glutamate control slope values, and plotted using XLfit (ID Business Solutions Ltd) to generate concentration–response curves. Potencies were calculated from fits using a four-point parameter logistic equation.

## APPENDIX A

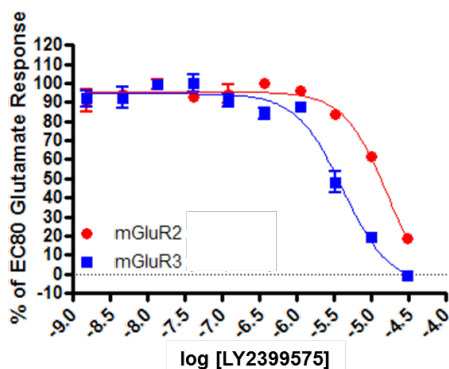
### REFERENCES CITED

1. Conn, P.J., et al., *Trends in Pharm. Sci.* **2008**, *30*, 25-31.
2. Fell, M.J., et al. *Neuropharmacology*. **2012**, *62*, 3.
3. Lindsley, C. W.; Shipe, W. D.; Wolkenberg, S. E.; Theberge, C. R.; Williams, D. L., Jr.; Sur, C.; Kinney, G. G. *Curr. Top. Med. Chem.* **2006**, *8*, 771.
4. Meltzer, H. Y. *Biol. Psychiatry*. **1999**, *46*, 1321.
5. Harrison, P.J.; Lyon, L.; Burnet, Pwj.; Lane, T.A. *J. Psychopharmacology*. **2008**, *22*, 308-322.
6. Hollmann, M.; Heinemann, S. *Annu. Rev. Neurosci.* **1994**, *17*, 31.
7. Conn, P.J.; Pin, J-P. *Annu. Rev. Pharmacol. Toxicol.* **1997**, *37*, 205-237.
8. Melancon, B.J.; Hopkins, C.R.; Wood, M.R.; Emmitte, K.A.; Niswender, C.M.; Christopoulos, A.; Conn, P.J.; Lindsley, C.W. *J. Med. Chem.* **2012**, *55*, 1445-1464.
9. Conn, P.J.; Duvoisin, R. *Neuropharmacology*. **1995**, *34*, 1.
10. Muto, T., et al. *PNAS*. **2007**, *104*, 3759-64.
11. Thathia, A.; Strooper, B.D.; *Nature Reviews Neuroscience*. **2011**, *12*, 73-87.
12. Conn, P.J.; Christopoulos, A.; Lindsley, C.W. *Nature Reviews Drug Discovery* **2009**, *8*, 41-54.
13. Conn, P.J.; Lindsley, C.W.; Jones, C. *Trends in Pharm. Sci.* **2009**, *30*, 25-31.
14. Robichaud, A.J.; Engers, D.W.; Lindsley, C.W.; Hopkins, C.R. *ACS Chem. Neurosci.* **2011**, *2*, 433-449.
15. Sheffler, D.J.; Pinkerton, A.B.; Dahl, R.; Markou, A.; Cosford, N.D.P. *ACS Chem. Neurosci.* **2011**, *2*, 382-393.
16. Owen, D.R. *ACS Chem. Neurosci.* **2011**, *2*, 394-401.

17. Emmitte, K.A. *ACS Chem. Neurosci.* **2011**, *2*, 443-449.
18. Stauffer, S.R. *ACS Chem. Neurosci.* **2011**, *2*, 450-470.
19. Harrision, P.J.; Lyon, L.; Sartorius, L.J.; Burnet, P.W.J.; Lane, T.A. *J. Psychopharm.* **2008**, *22*, 308-322.
20. Kew, JNC; Kemp, J.A. *Psychopharmacology* **2005**, *179*, 4-29.
21. Woltering, T.J.; Wichmann, J.; Goetschi, E.; Knoflach, F.; Ballard, T.M.; Huwyler, J.; Gatti, S. *Bioorg. Med. Chem. Lett.* **2010**, *20*, 6969-6974.
22. Corti, C.; Battaglia, G.; Molinaro, G.; Riozzi, B.; Pittaluga, A.; Corsi, M.; Mugnaini, M.; Nicoletti, F.; Bruno, V. *J. Neurosci.* **2007**, *27*, 8297-8308.
23. Moghaddam, B.; Adams, B.W. *Science* **1998**, *281*, 1349-1352.
24. Matrisciano, F.; Panaccione, I.; Zusso, M.; Giusti, P.; Tatarelli, R.; Iacovelli, L.; Mathe, A.A.; Gruber, S.H.; Nicoletti, F.; Girardi, P. *Mol. Psychiatry* **2007**, *12*, 704-706.
25. Markou, A. *Biol. Psychiatry* **2007**, *61*, 17-22.
26. Varney, M.A.; et al. *The Journal of Pharmacology and Experimental Therapeutics.* **1999**, *290*, 170-81.
27. O'Leary, D.M.; Movsesyan, V.; Vicini, S.; Faden, A.I. *British journal of pharmacology* **2000**, *131*, 1429-37.
28. Cosford, N.D.; Tehrani, L.; Roppe, J.; et al. *J. Med. Chem.* **2003**, *46*, 204-206.
29. Williams, R.; Manka, J.T.; Rodriguez, A.L.; Vinson, P.N.; Niswender, C.M.; Weaver, C.D.; Jones, C.K.; Conn, P.J.; Lindsley, C.W.; Stauffer, S.R. *Bioorg. Med. Chem. Lett.* **2011**, *21*, 1350-1353.
30. Rodriguez, A.L.; Grier, M.D.; Jones, C.K.; Herman, E.J.; Kane, A.S.; Smith, R.L.; Williams, R.; Zhou, Y.; Marlo, J.E.; Days, E.L.; Blatt, T.N.; Jadhav, S.; Menon, U.; Vinson, P.N.; Rook, J.M.; Stauffer, S.R.; Niswender, C.M.; Lindsley, C.W.; Weaver, C.D.; Conn, P.J. *Mol. Pharm.* **2010**, *78*, 1105-1123.
31. Ritzen, A.; Sindet, R.; Hentzer, M.; Svendsen, N.; Brodbeck, R.M.; Bungaard, C. *Bioorg. Med. Chem. Lett.* **2009**, *19*, 3275-3278.
32. Wood, M.R.; Hopkins, C.R.; Brogan, J.T.; Conn, P.J.; Lindsley, C.W. *Biochemistry* **2011**, *50*, 2403-2410.



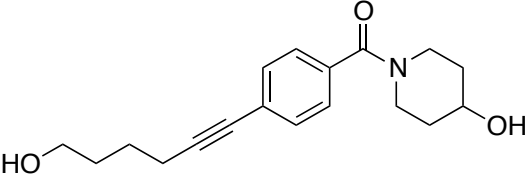
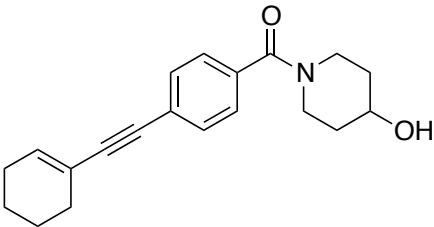
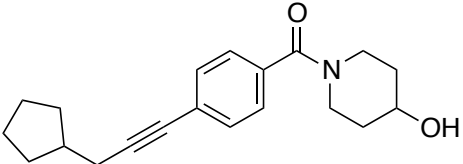
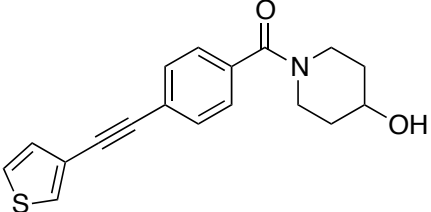
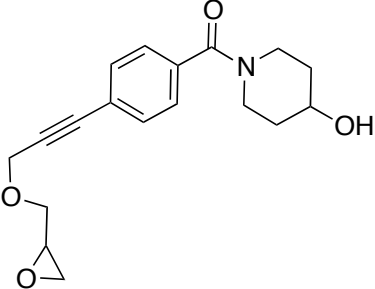
33. Campo, B.; Kalinichev, M.; Lambeng, N.; El Yacoubi, M.; Royer-Urios, I.; Schneider, M.; Legarnd, C.; Parron, D.; Girard, F.; Bessif, A.; Poli, S.; Vaugeois, J-M.; Le Poul, E.; Celanire, S. *J. Neurogenetics* **2011**, *24*, 152-166.
34. Caraci, F.; Molinaro, G.; Battaglia, G.; Giuffrida, M.L.; Rizzo, B.; Traficante, A.; Bruno, V.; Cannella, M.; Mero, S.; Wang, X.; Heinz, B.A.; Nisenbaum, E.S.; Britton, T.C.; Drago, F.; Sortino, M.A.; Copani, A.; Nicoletti, F. *Mol. Pharm.* **2011**, *79*, 618-626
35. CRCs for LY2389575 (**2**) in our GIRK assays:

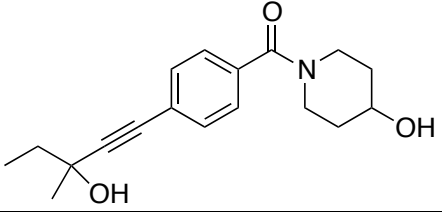
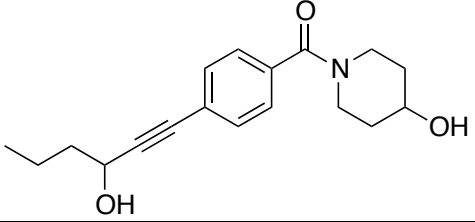
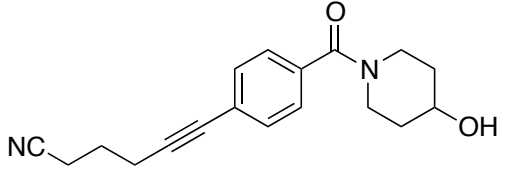
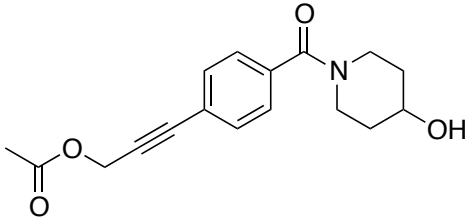
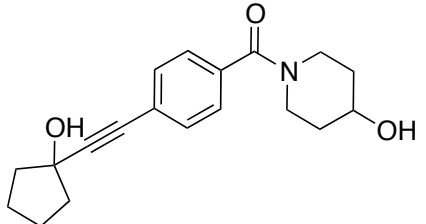
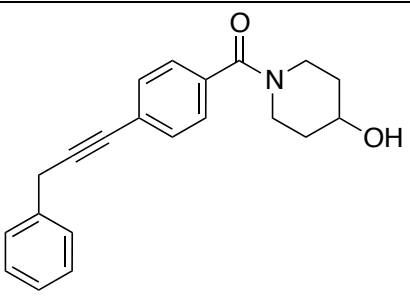
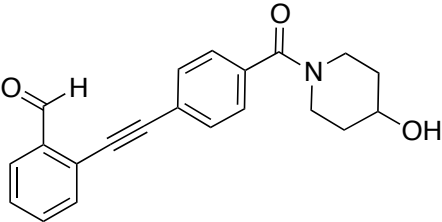


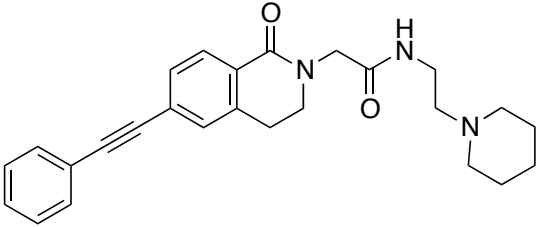
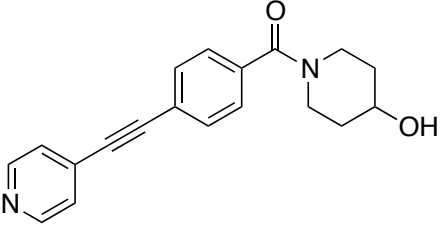
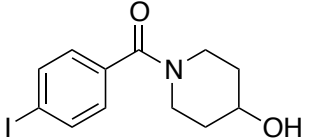
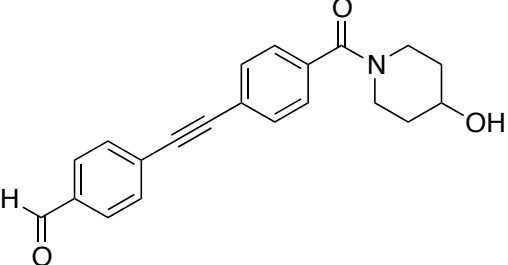
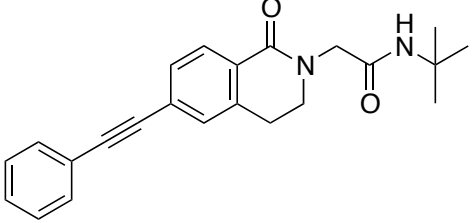
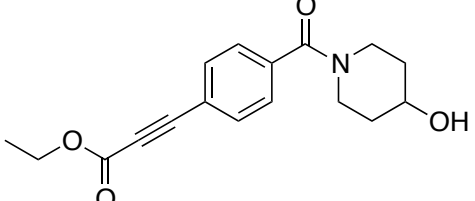
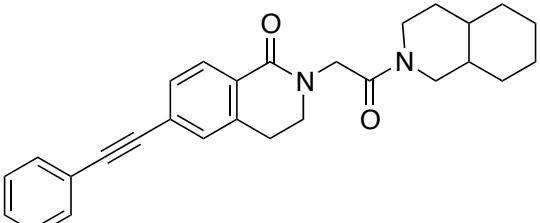
36. Sharma, S.; Rodriguez, A.; Conn, P.J.; Lindsley, C.W. *Bioorg. Med. Chem. Lett.* **2008**, *18*, 4098-4101.
37. Sharma, S.; Kedrowski, J.; Rook, J.M.; Smith, J.M.; Jones, C.K.; Rodriguez, A.L.; Conn, P.J.; Lindsley, C.W. *J. Med. Chem.* **2010**, *52*, 4103-4106.
38. Brodbeck, B.; et al. *Tet. Lett.* **2003**, *44*, 1675-1678.
39. Leister, W.H.; Strauss, K.A.; Wisnoski, D.D.; Zhao, Z.; Lindsley, C.W. *J. Comb. Chem.* **2003**, *5*, 322-329.
40. Niswender, C.M.; Johnson, K.A.; Luo, Q.; Ayala, J.E.; Kim, C.; Conn, P.J.; Weaver, C.D.; *Mol. Pharm.* **2008**, *73*, 1213-1224.
41. For full information on the targets in the Lead Profiling Screen at Ricerca, please see: [www.ricerca.com](http://www.ricerca.com)
42. Urwyler, S. *Pharmacol Rev.* **2011**, *63*, 59-126.

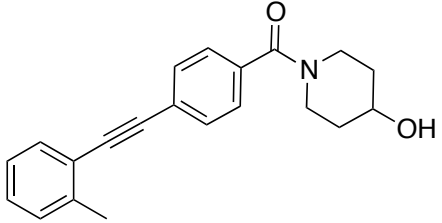
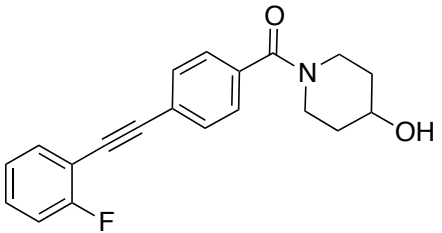
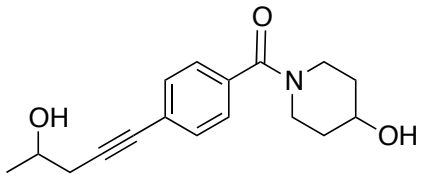
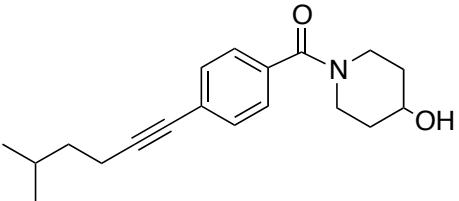
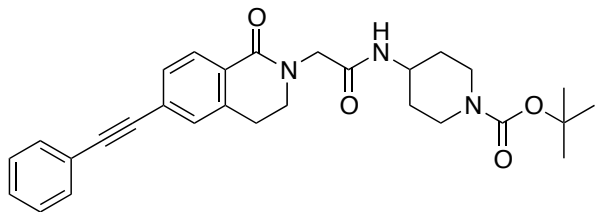
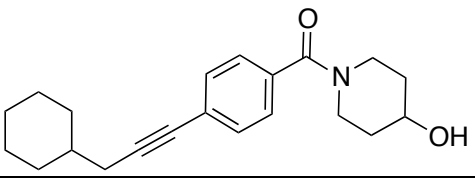
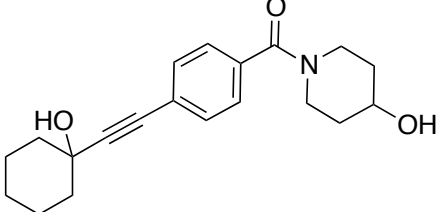
## APPENDIX B

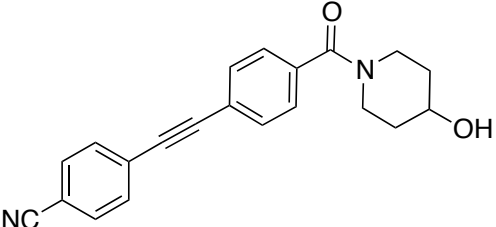
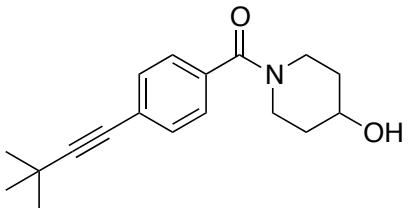
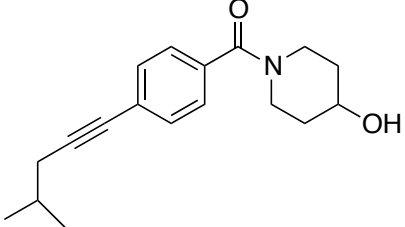
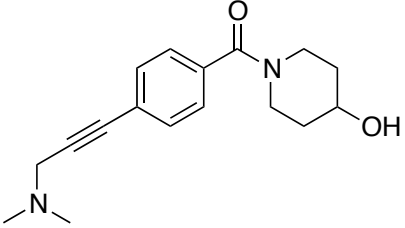
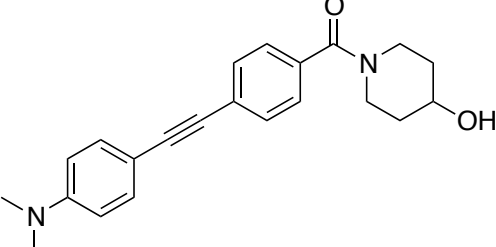
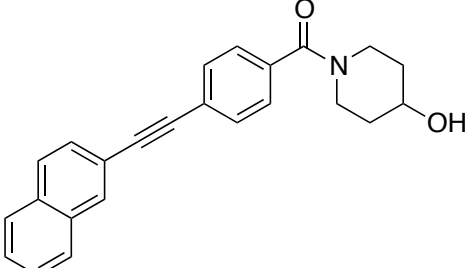
### COMPOUND STRUCTURES

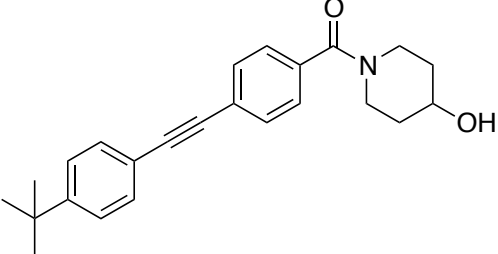
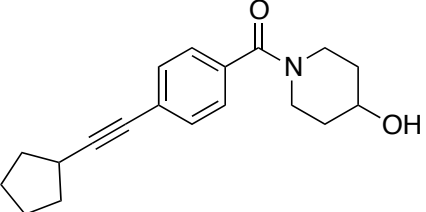
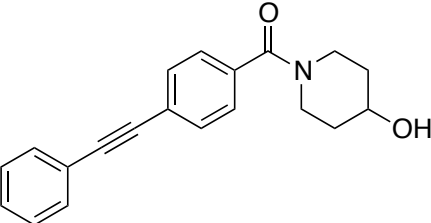
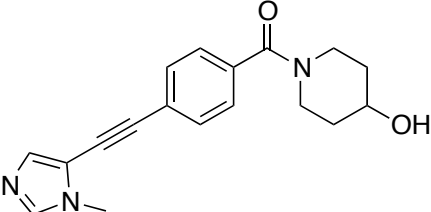
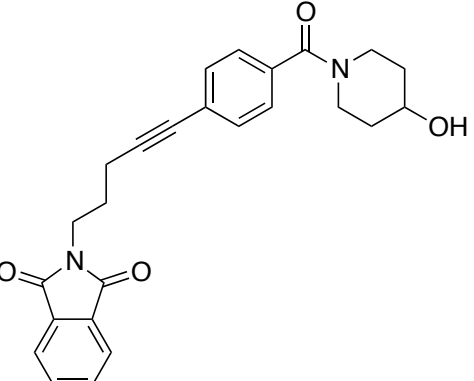
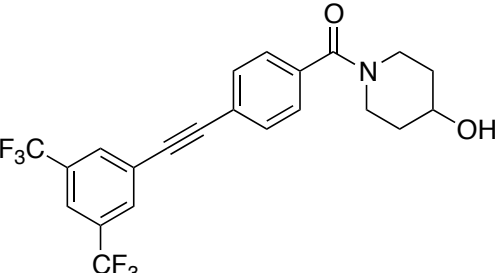
Structure	VU #	Notebook Reference
	VU0457496	CJW-1-35-104
	VU0457497	CJW-1-35-107
	VU0457498	CJW-1-38-115
	VU0457499	CJW-1-35-108
	VU0457500	CJW-1-38-116

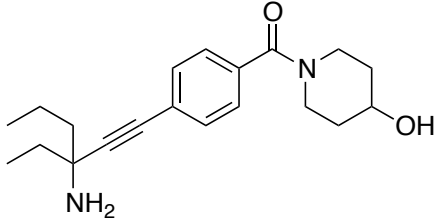
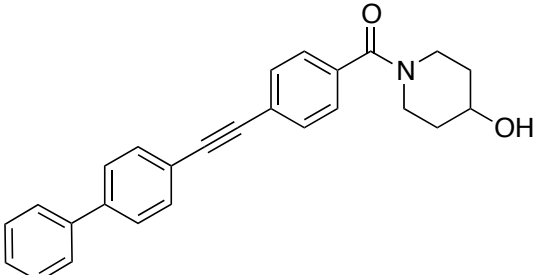
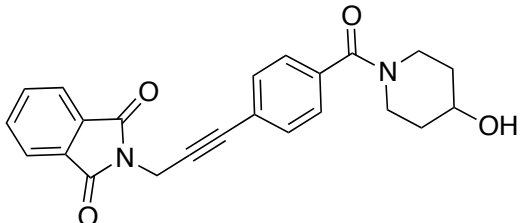
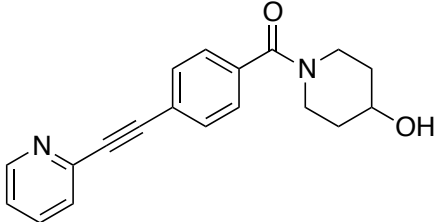
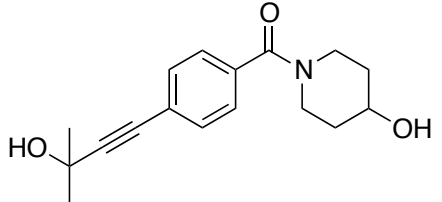
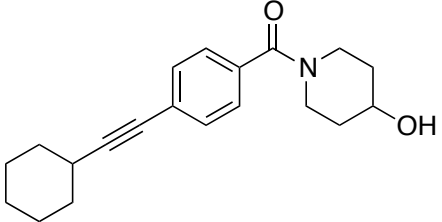
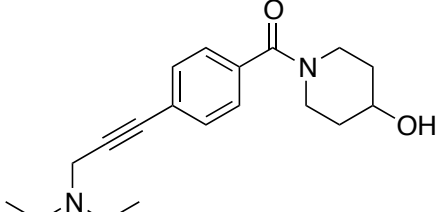
	VU0457501	CJW-1-35-105
	VU0457502	CJW-1-35-106
	VU0457503	CJW-1-33-100
	VU0457504	CJW-1-35-103
	VU0457505	CJW-1-38-117
	VU0457506	CJW-1-38-118
	VU0457507	CJW-1-40-129

	VU0402207	CJW-1-32-97
	VU0402219	CJW-1-37-112
	VU0457508	CJW-1-12-1
	VU0457509	CJW-1-37-111
	VU0457510	CJW-1-36-109
	VU0457511	CJW-1-37-110
	VU0457512	CJW-1-39-121

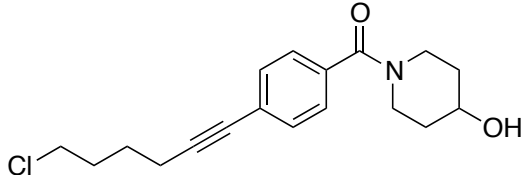
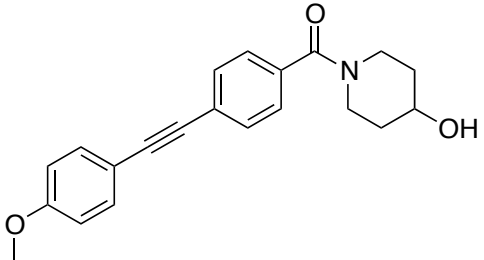
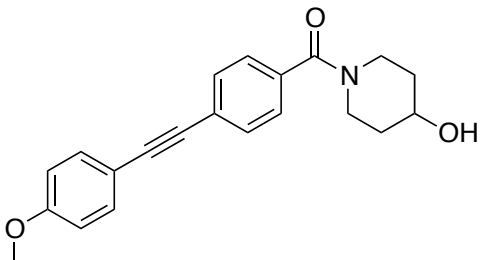
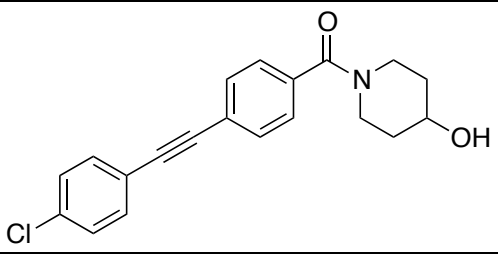
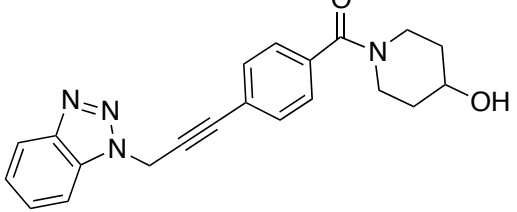
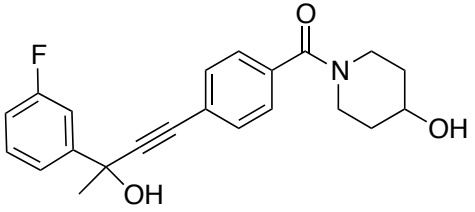
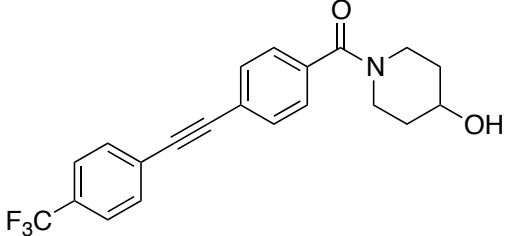
	VU0457513	CJW-1-40-124
	VU0402215	CJW-1-40-125
	VU0457514	CJW-1-33-99
	VU0457515	CJW-1-33-101
	VU0457516	CJW-1-41-130
	VU0457517	CJW-1-40-126
	VU0457518	CJW-1-40-127

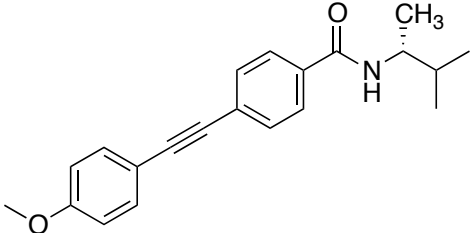
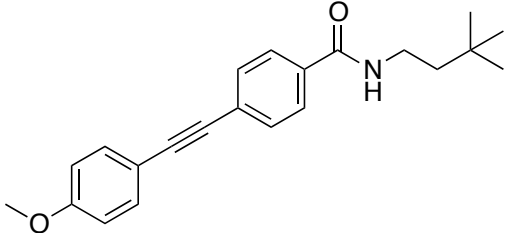
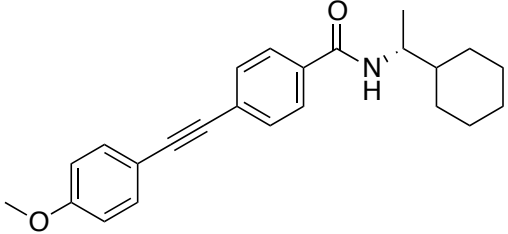
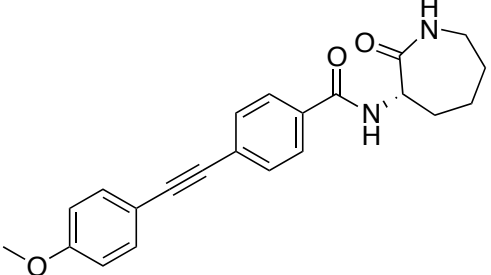
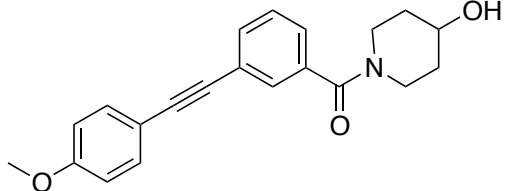
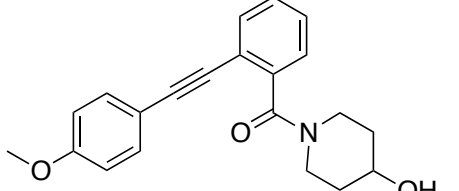
	VU0457519	CJW-1-40-128
	VU0402211	CJW-1-14-5
	VU0457286	CJW-1-15-6
	VU0457287	CJW-1-16-7
	VU0457288	CJW-1-20-23
	VU0402220	CJW-1-20-24

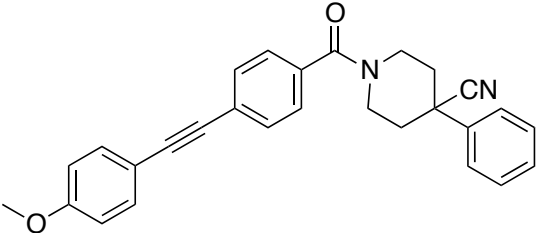
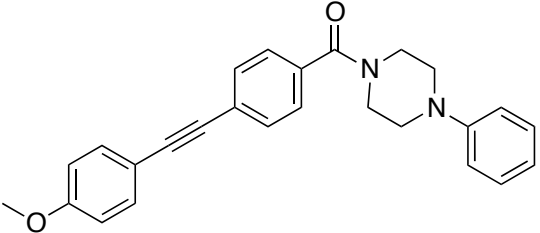
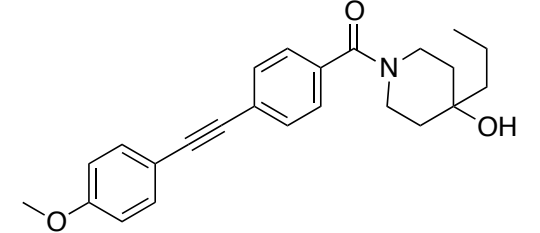
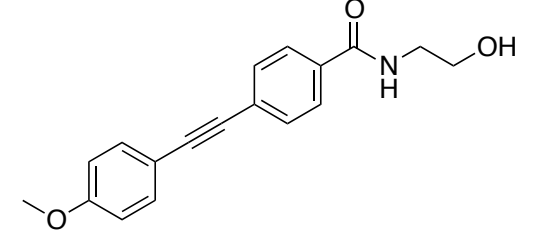
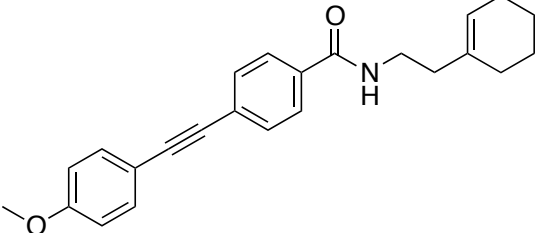
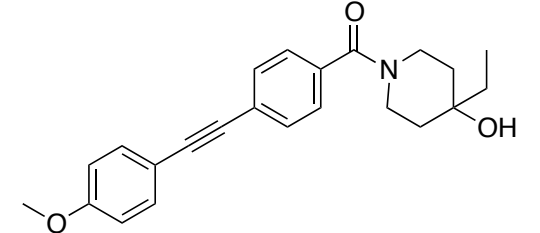
	VU0457289	CJW-1-20-26
	VU0457290	CJW-1-17-9
	VU0092273	CJW-1-18-11
	VU0457291	CJW-1-18-13
	VU0457292	CJW-1-22-31
	VU0457293	CJW-1-22-32

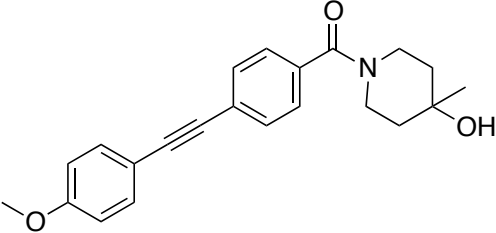
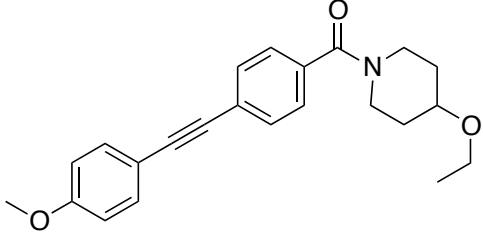
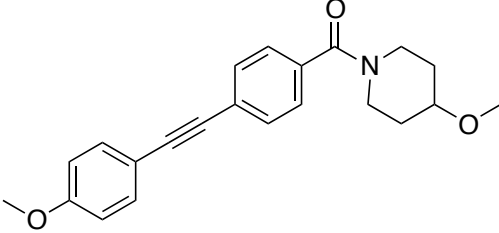
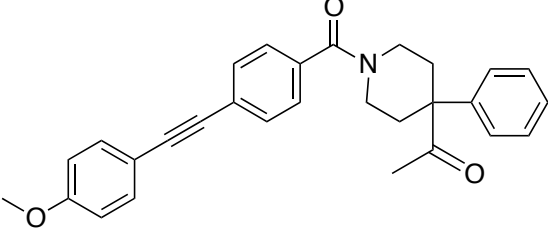
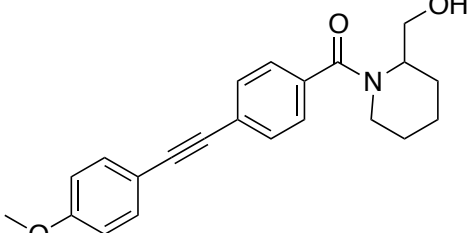
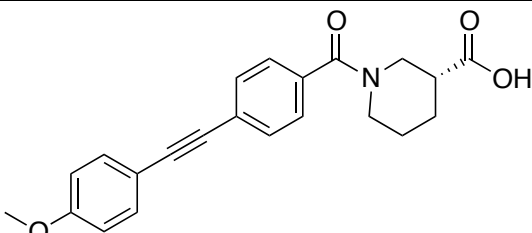
	VU0457294	CJW-1-22-35
	VU0457295	CJW-1-21-29
	VU0457296	CJW-1-22-30
	VU0402212	CJW-1-18-12
	VU0402226	CJW-1-17-8
	VU0402214	CJW-1-18-14
	VU0457297	CJW-1-19-15

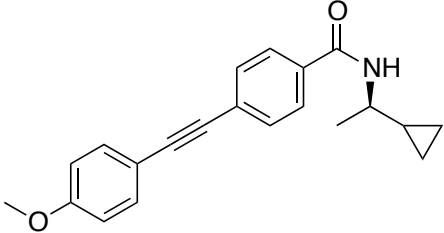
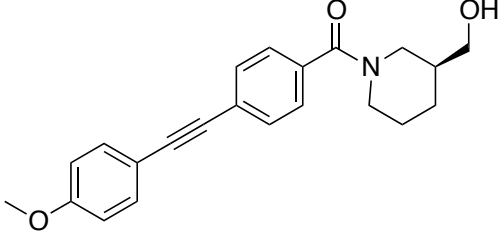
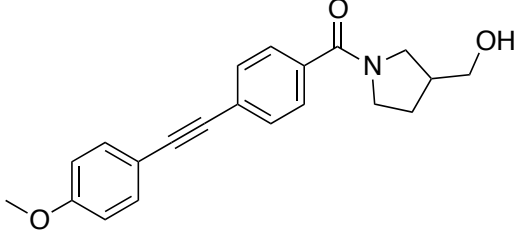
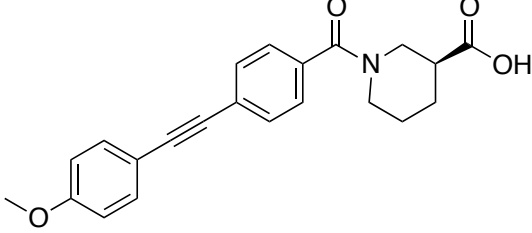
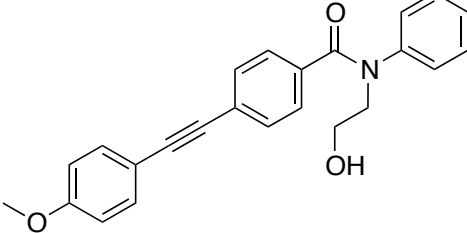
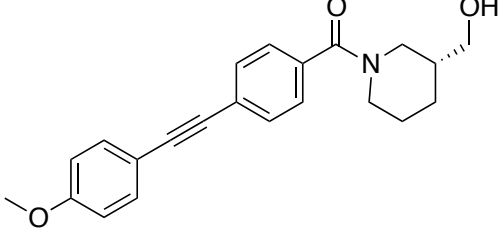


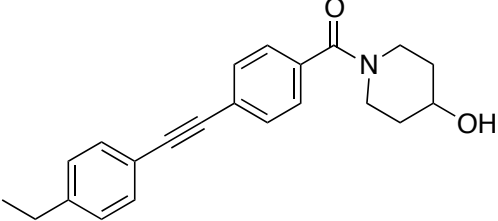
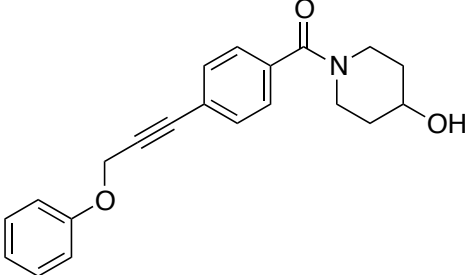
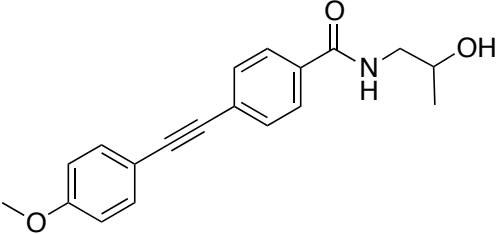
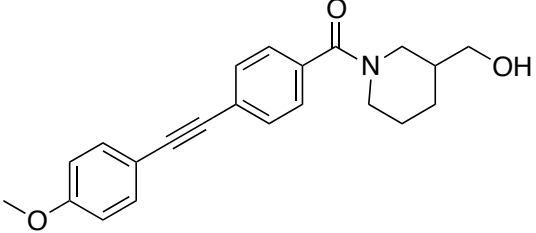
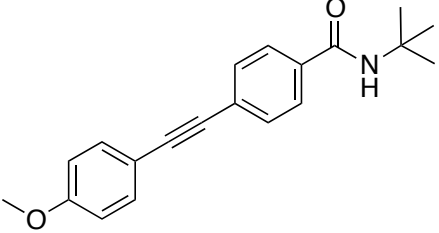
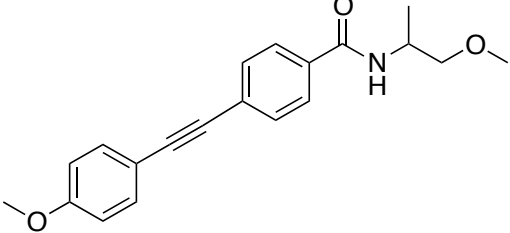
	VU0457298	CJW-1-19-16
	VU0457299	CJW-1-19-18
	VU0457299	JAB-2-15-1
	VU0457300	CJW-1-20-20
	VU0457301	CJW-1-20-25
	VU0457302	CJW-1-21-27
	VU0402222	CJW-1-21-28

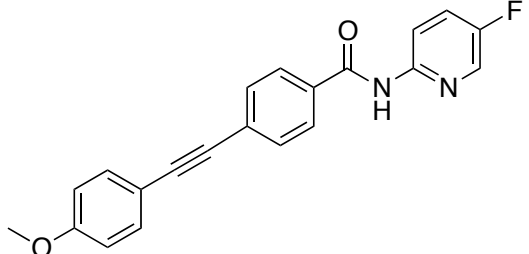
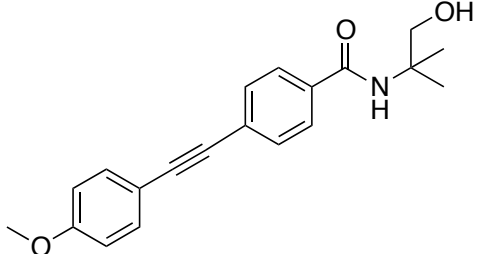
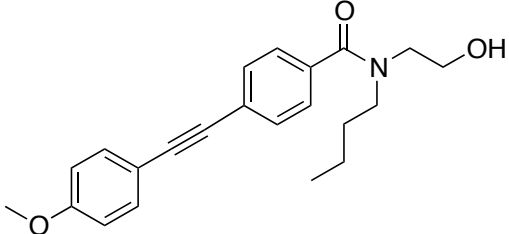
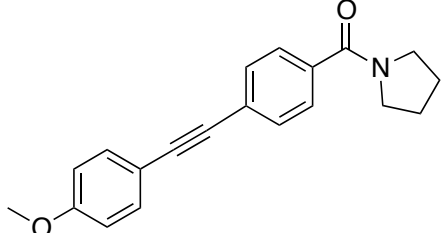
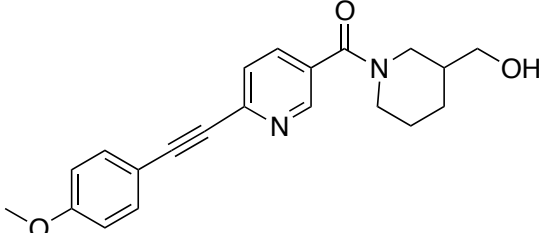
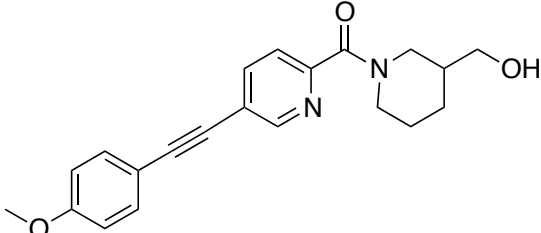
	VU0459886	CJW-1-58-158
	VU0459887	CJW-1-58-157
	VU0461407	JAB-1-81-A69
	VU0461452	CJW-1-59-160
	VU0461485	CJW-1-63-166
	VU0461486	CJW-1-66-169

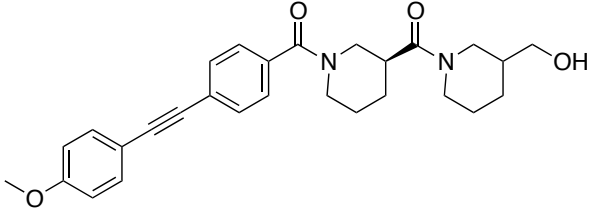
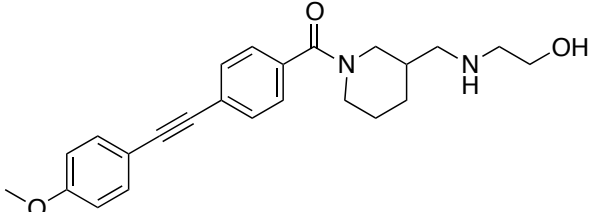
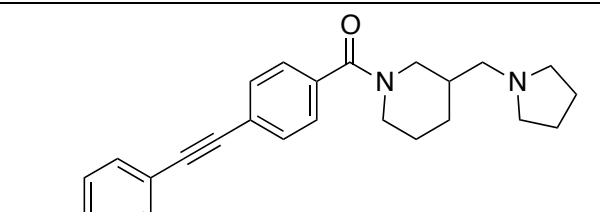
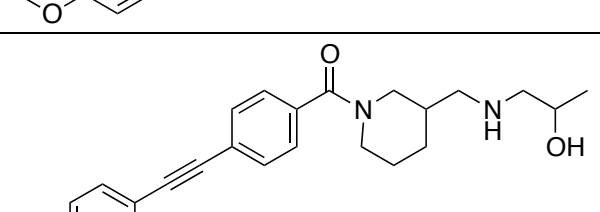
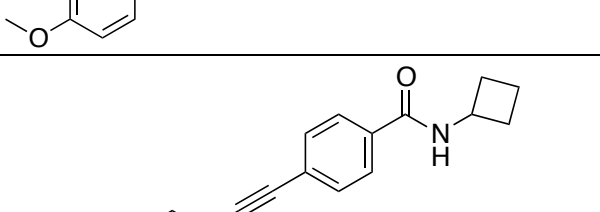
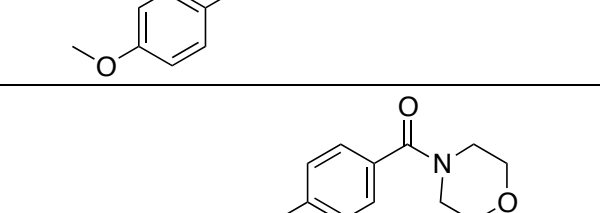
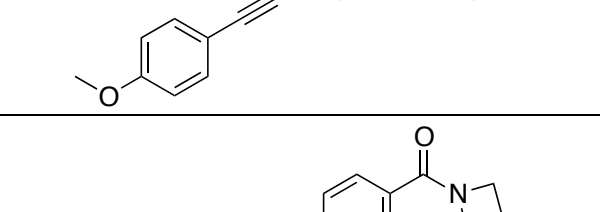
	VU0461487	CJW-1-59-161
	VU0461488	CJW-1-59-162
	VU0462506	JAB-1-97-1
	VU0462507	JAB-1-101-A19
	VU0462508	JAB-1-101-A4
	VU0462509	JAB-1-96

	VU0462510	JAB-1-104
	VU0462511	JAB-1-107-1
	VU0461495	JAB-1-89
	VU0461496	CJW-1-59-159
	VU0463590	JAB-1-112-1
	VU0463591	JAB-1-112-4

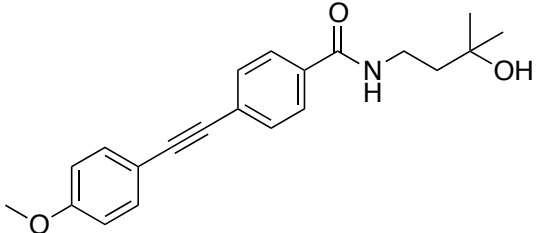
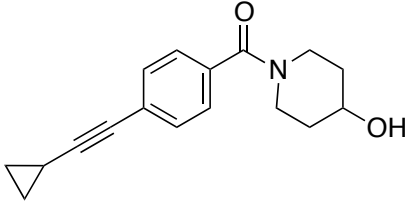
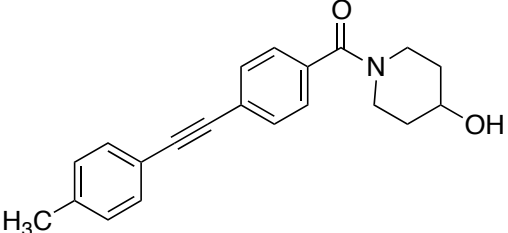
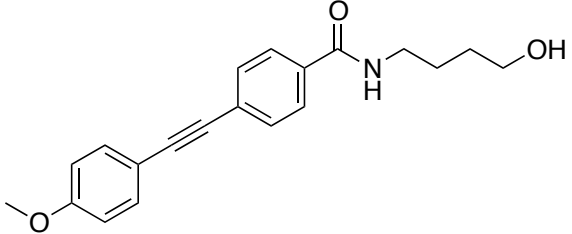
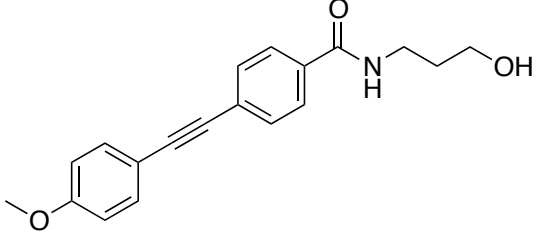
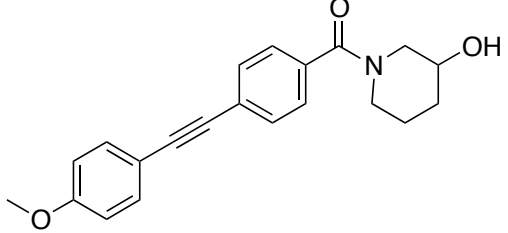
	VU0463592	JAB-1-114-6
	VU0463593	JAB-1-116-S
	VU0463594	JAB-1-112-2
	VU0463595	JAB-1-112-3
	VU0463596	JAB-1-114-4
	VU0463597	JAB-1-116-R

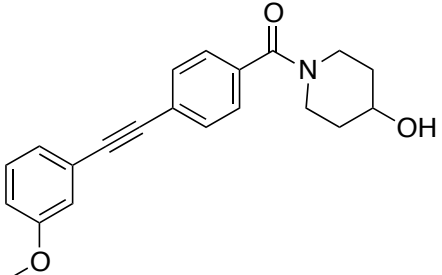
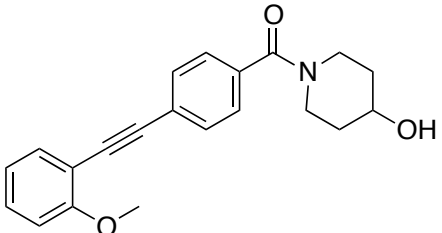
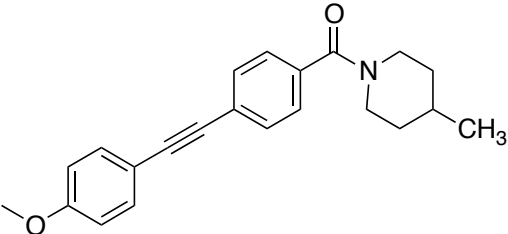
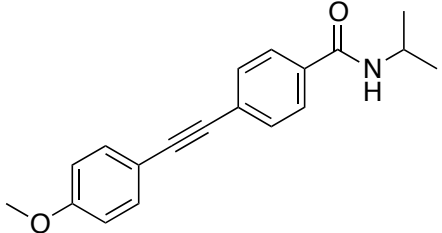
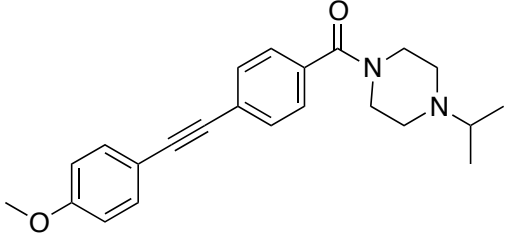
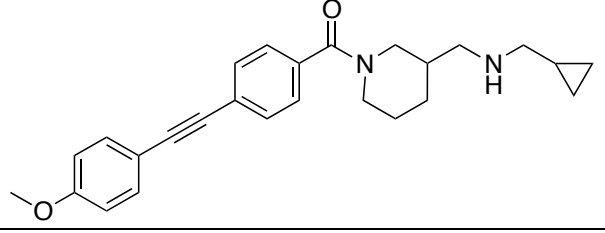
	VU0458690	CJW-1-43-133
	VU0458691	CJW-1-43-136
	VU0459725	JAB-1-81-A31
	VU0459726	JAB-1-81-A43
	VU0459727	JAB-1-84-1
	VU0459728	JAB-1-84-2

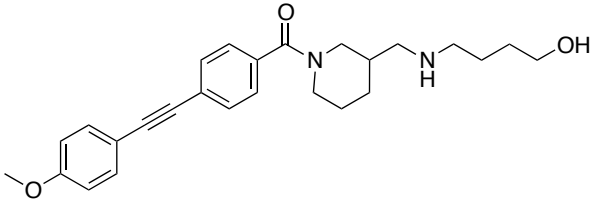
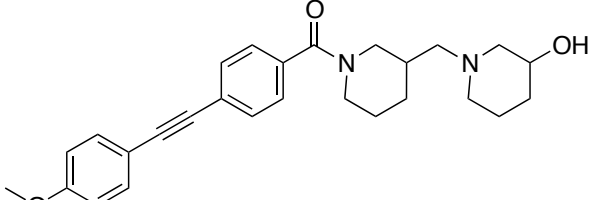
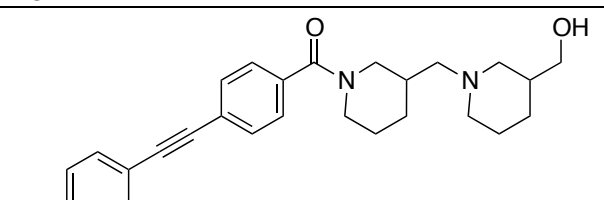
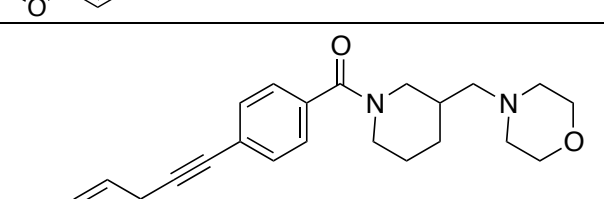
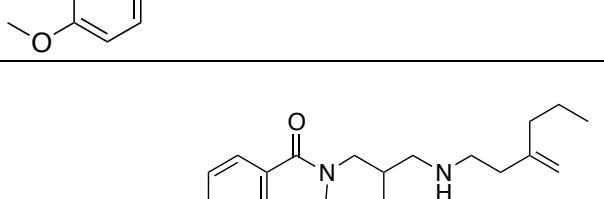
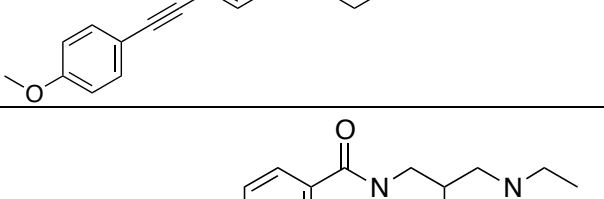
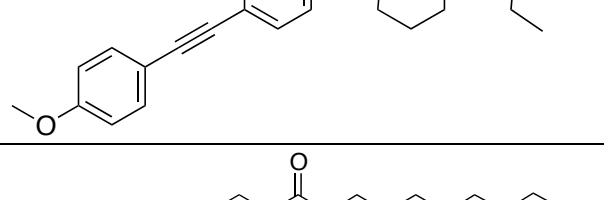
	VU0459729	JAB-1-84-3
	VU0459730	JAB-1-84-5
	VU0459731	JAB-1-84-4
	VU0459732	JAB-1-78-A2
	VU0464192	JAB-1-127
	VU0464193	JAB-1-135

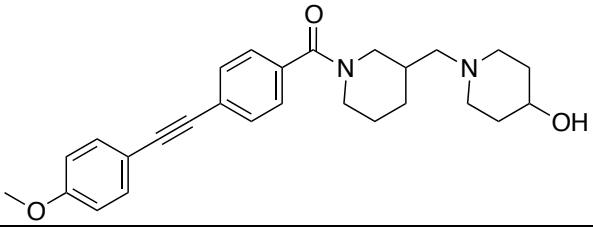
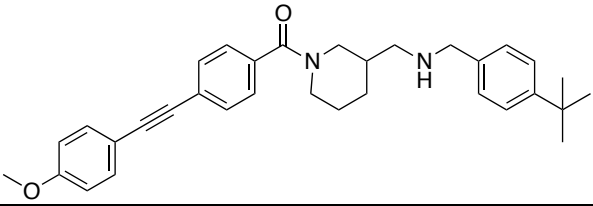
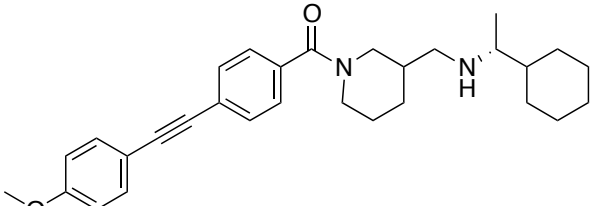
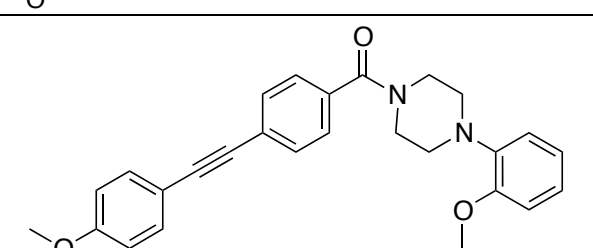
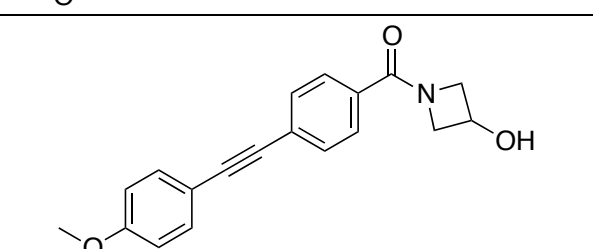
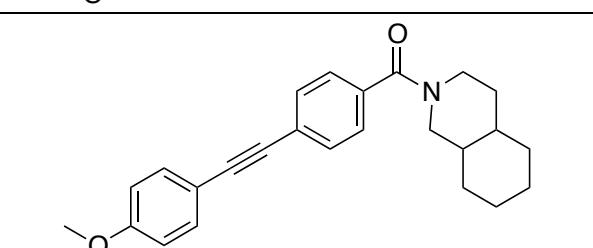
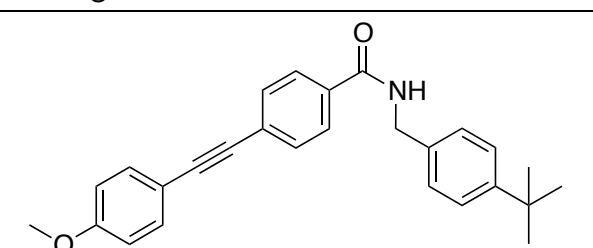
	VU0464194	JAB-1-125-RA43
	VU0464195	JAB-1-136
	VU0464678	JAB-1-139-1
	VU0464679	JAB-1-139-2
	VU0459800	CJW-1-57-151
	VU0459801	JAB-1-122-1
	VU0459802	CJW-1-57-154

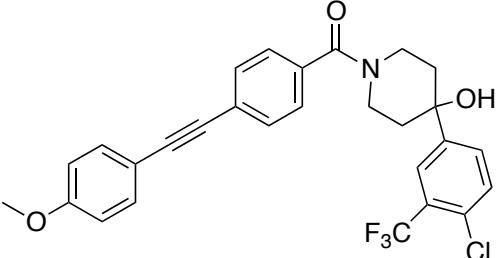
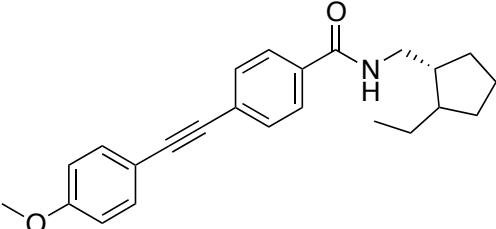
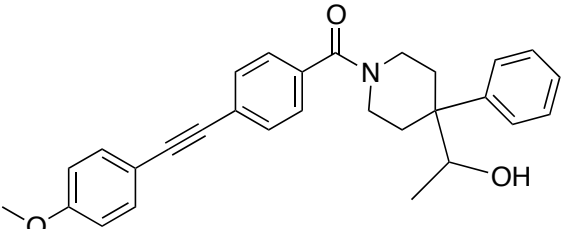
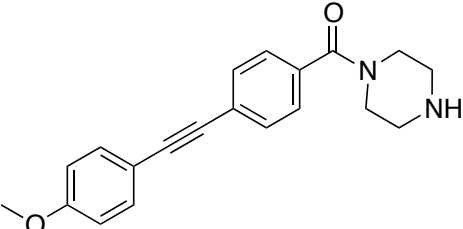
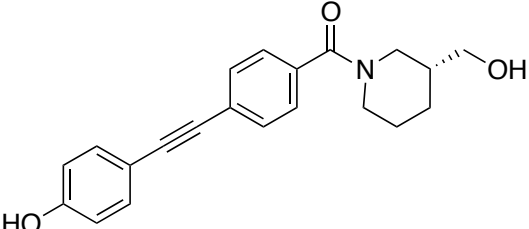
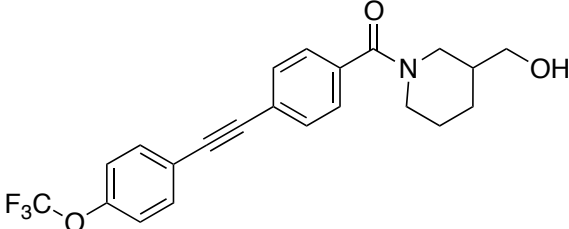


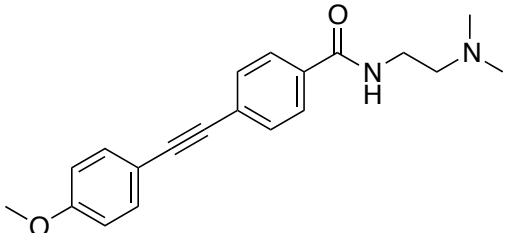
	VU0459803	CJW-1-57-155
	VU0459804	CJW-1-46-138
	VU0459805	CJW-1-46-139
	VU0459806	CJW-1-47-144
	VU0459807	CJW-1-47-143
	VU0459808	CJW-1-49-147

	VU0459809	CJW-1-46-140
	VU0459810	CJW-1-46-141
	VU0459811	CJW-1-47-142
	VU0459812	CJW-1-49-146
	VU0459813	CJW-1-49-148
	VU0464718	JAB-2-1-3

	VU0464719	JAB-2-1-9
	VU0464720	JAB-2-1-12
	VU0464721	JAB-1-139-3
	VU0464722	JAB-2-1-1
	VU0464723	JAB-2-1-4
	VU0464724	JAB-2-1-5
	VU0464725	JAB-2-1-7

	VU0464726	JAB-2-1-13
	VU0464727	JAB-2-1-14
	VU0464728	JAB-2-1-15
	VU0459814	CJW-1-49-149
	VU0459815	CJW-1-57-156
	VU0459816	JAB-1-81-A45
	VU0459817	JAB-1-81-A66

	VU0459818	JAB-1-81-A68
	VU0459819	JAB-1-81-A61
	VU0463824	JAB-1-120
	VU0463825	JAB-1-122-2
	VU0465634	JAB-2-20
	VU0465635	JAB-2-23

 <chem>CN(C)CCNC(=O)c1ccc(cc1)C#Cc2ccc(OC)cc2</chem>	VU0465636	JAB-2-15-5
---	-----------	------------